Marine and terrestrial proxy records of environmental changes across the Triassic/Jurassic transition:

A combined geochemical and palynological approach

Master thesis

Martin A. N. Schobben
Supervised by
Wolfram M. Kürschner[1]; Gert-Jan Reichart[2]

University Utrecht
1) Department of Biology - Palaeoecology group
2) Department of Earth sciences - Organic geochemistry group

Abstract

The Triassic–Jurassic boundary (~ 201.58 Ma; Schaltegger et al., 2008) represent a period of mass extinction. The occurrence of intense volcanic activity (Central Atlantic Magmatic Province or CAMP) and global carbon cycle perturbations is thought to be responsible for the extinction. The negative carbon isotopic excursions found at the end- Triassic suggests that large amounts of carbon were released by possibly marine methane hydrate reservoirs, possibly destabilized by CAMP and associated warming. Similarly to previous studies our results confirm the existence of two profound warming events, with the first warming pulse correlating with an episode of intense volcanism. However the new data is obtained via a geochemical and palynological approach, respectively with foraminiferal tests and palynomorphs, instead of a single proxy.

1 Introduction

The end-Triassic mass extinction is marked by up to 50% marine biodiversity loss (Raup & Sepkoski, 1982). However the exact impact on terrestrial diversity is less well constrained. In the Newark basin (USA) a decline of 60% of the palynomorph taxa has been recorded, followed by a spore-spike at the T-J boundary, which has been interpreted as a mass extinction (Fowell & Olsen, 1993; Fowell et al., 1994; Olsen et al., 2002a). A number of European sections, however, show gradual changes within the palynomorph assemblages (Bonis et al., 2009; Bonis, Ruhl, & Kürschner, 2010b; Hounslow, Posen, & Warrington, 2004a; Hounslow, Posen, & Warrington, 2004b; Kürschner et al., 2007) and a gradual extinction within plant macrofossil assemblages has been reported from a Greenland section (McElwain et al., 2007).

The Late Triassic is furthermore marked by the short and pronounced initial negative carbon isotopic excursion (CIE) and the long-lasting but less pronounced main CIE. The initial CIE was first recognized in Total Organic Carbon (TOC) at various sites globally (Hesselbo et al., 2002; Pálfy et al., 2001; M. Ruhl et al., 2009; Ward et al., 2001). Additionally, Galli et al., (2005) and Pálfy et al., (2001), observed the initial CIE in bulk calciumcarbonate and more recently also in carbon isotopes of long chain *n*-alkanes from epicuticilar waxes of land plants (M. Ruhl et al., in prep.). Both CIE's have been found in the TOC of several European sections (Hesselbo et al., 2002; Kürschner et al., 2007; M. Ruhl et al., 2009) and within $\delta^{13}C$ of calciumcarbonate of oysters from the UK (Korte et al., 2009).

Since the carbon isotopic composition of *n*-alkanes, reflect the isotopic composition of atmospheric CO_2, the initial CIE has been assumed to reflect a real C-cycle perturbation. It has therefore been proposed that dissociation of isotopically depleted marine methane clathrates ($\delta^{13}C$ values of -60 ‰) can explain; the magnitude (6 ‰ inferred from the $\delta^{13}C_{\ n\text{-alkanes}}$) and especially the short duration (20-40 kyr) of the initial CIE (Beerling & Berner, 2002; M. Ruhl et al., in prep.). Destabilization of marine methane clatherates could be the result of seawater warming due to CO_2 outgassing of CAMP (Figure 1). This two-step release of greenhouse gasses, caused severe climate changes, which have been confirmed by quantitative changes in palynomorph assemblages of the Hochalplgraben, Kuhjoch (Austria) (Bonis & Kürschner in prep. a) and st. Audrie's Bay (UK) (Bonis & Kürschner, in prep. b). Korte et al. (2009) reported a

warming of the climate during the onset of the main CIE, inferred from an oxygen isotope record of oyster shells, from Lavernock point (UK). So similar mechanisms as previously proposed, could apply for the main CIE (Bonis & Kürschner, in prep. b). Anoxia and acidification of especially restricted marine basins were possibly responsible for stress and deterioration in marine ecosystems (Bonis, Ruhl, & Kürschner, 2010a; Hautmann, 2004; Hautmann et al., 2008)

The Kuhjoch section (Tr-J Global Stratotype Section and Point) contains an almost continues sedimentary sequence with an extensive marine and terrestrial fossil record, hence the section is ideal for a multi-proxy study, dealing with the environmental and climate changes associated with the end-Triassic CIE's. The resolution and extend of the palynological record will be increased when compared with previous studies (Bonis & Kürschner, in prep. a; Bonis et al., 2009), and used for multivariate analyses which quantify changes in the palynomorph record, possibly associated with environmental or climatic change. Furthermore foraminiferal shells of Kuhjoch will be chemically analyzed, because of their possibly good preservation (A. v. Hillebrandt & Urlichs, 2008) and the successful use of foraminiferal shells as proxies in both paleooceanographic and paleoclimatic studies (Chave, 1954; Emiliani, 1955; Nürnberg et al., 1996; Shackleton & Opdyke, 1973; Shackleton & Opdyke, 1973). The isotopic ratios of C and O in calciumcarbonate shells of foraminifera are known to reflect to a great extent the C and O isotopic ratios of the ambient seawater. Although some processes (e.g. vital effects, migration, microhabitat effect, ontogenic effects and changing carbonate ion concentrations) do cause deviations (Rohling & Cooke, 2003), however they are probably minor when compared with climatically induced changes over long timescales (Korte et al., 2009) and the possibility of a diagenetic overprint due to the extended period of burial. When further analyses rule out any chemical alteration of the calciumcarbonate, the foraminiferal shells together with the palynomorphs could be excellent proxies for environmental and climatic changes of both the terrestrial and marine realm at the Tr-J boundary interval.

2 Background

End Triassic climate change and mass extinctions

The bulk organic carbon isotopic record of Kuhjoch is marked by two negative CIE's, one sharp pronounced shift with an short duration (initial CIE) at the base of the Kendlbach formation followed by a longer lasting but less pronounced shift (main CIE) starting at the top of the Schattwald beds (Figure 3) (Ruhl et al., 2009). The initial CIE has been described in different sections around the world (Galli et al., 2005; Pálfy et al., 2001; Ward et al., 2007; Williford et al., 2007) and sections containing both the initial and main CIE have also been described (Hesselbo et al., 2002; Kürschner et al., 2007; M. Ruhl et al., 2009). Therefore it has been assumed that these negative CIE's mark real perturbations of the global carbon cycle of the End-Triassic. The initial CIE within Kuhjoch is furthermore marked by little change in the organic matter composition revealed by Rock- Eval analyses (M. Ruhl et al., 2010) and additionally it has been documented in C-isotopes from long chain *n*-alkanes with a strong odd over even predominance, which are the molecular remnants of epicuticular plant waxes (M. Ruhl et

al., in prep.). This $\delta^{13}C_{\ n\text{-alkanes}}$ record directly reflects changes of atmospheric $\delta^{13}C$, since the carbon is derived from the atmosphere during photosynthesis (M. Ruhl et al., in prep.). McElwain et al. (2007) additionally, put forward evidence for a potential fourfold increase in atmospheric CO_2 concentrations during the end-Triassic, based on stomatal density of fossil leaves.

This led to the assumption that an atmospheric injection of light carbon caused the CIE's, possibly by CO_2 outgassing from volcanism, dissociation of marine methane hydrates, or a combination of both (Hesselbo et al., 2002; Pálfy et al., 2001). Beerling & Berner (2002) and M. Ruhl et al. (in prep.) Furthermore proposed that the large magnitude of the C-cycle disruption (5-6 ‰ based on $\delta^{13}C_{n\text{-alkanes}}$) and especially its short duration (< 10 kyr for the onset solely), makes volcanism unlikely as the only source. Hence, isotopically very light methane (with a $\delta^{13}C$ of -60‰) is more likely the cause and with the use of a simple mass balance M. Ruhl et al., (in prep.), calculated that the release of ~ 6900-8200 Gt carbon in the form of CH_4 could explain the magnitude of the initial CIE. However this is higher than estimates of today's total marine methane hydrate reservoir (~3000 Gt), so possibly other sources of isotopically depleted carbon contribute to the observed CIE, e.g. sub surface combustion of organic rich strata by intrusive volcanism or thermogenic methane release by volcanism (Dunkley Jones et al., 2010). Furthermore the use of terrestrial organic records could also result in overestimation of the magnitude of the C-cycle disruption. Probably because similar amplification mechanism (e.g. soil cycling rates or relative humidity) as proposed for the PETM contributed to the magnitude of the terrestrial CIE (Bowen et al., 2004). Additionally vital effects, specific to the plant type can fractionate to a different extends e.g. for the PETM event, variability in $\delta^{13}C_{\ n\text{-alkanes}}$ values is partially caused by the composition of the vegetation (angiosperms vs. gymnosperms predominance) (Schouten et al., 2007). In the scenario of metastable methane hydrate, CO_2 outgassing of CAMP volcanism could have initiated the dissociation by warming of the oceans and thereby creating a runway greenhouse effect equivalent to the Perm/Triassic extinction events (Benton & Twitchett, 2003) (Figure 2). In the Argana section (Morocco), the initial CIE and a marine extinction event, have been linked to the first pulse of CAMP volcanism (Deenen et al., 2010).

This possibly large injection of carbon to the atmosphere would cause severe greenhouse conditions; hence climatic changes at the Tr-J boundary would have been profound. As has been observed with multivariate analyses on palynomorph records of Kuhjoch, Hochalplgraben (Austria) and St. Audries Bay (UK) (Bonis & Kürschner, in prep a; Bonis & Kürschner, in prep. b) and furthermore with a $\delta^{18}O$ record of biogenic calciumcarbonate from Lavernock point (UK) (Korte et al., 2009). Further consequences could have been rapid acidification of the oceans (Caldeira & Wickett, 2003; J. Zachos et al., 2005) and local anoxia due to enhanced runoff (Bonis, Ruhl, & Kürschner, 2010a). This acidification is likely to have caused a number of effects, particularly for marine calcifiers, and resulted in stress and deterioration of marine ecosystems and possibly responsible for the extinction of many marine species (Hautmann, 2004; Hautmann et al., 2008).

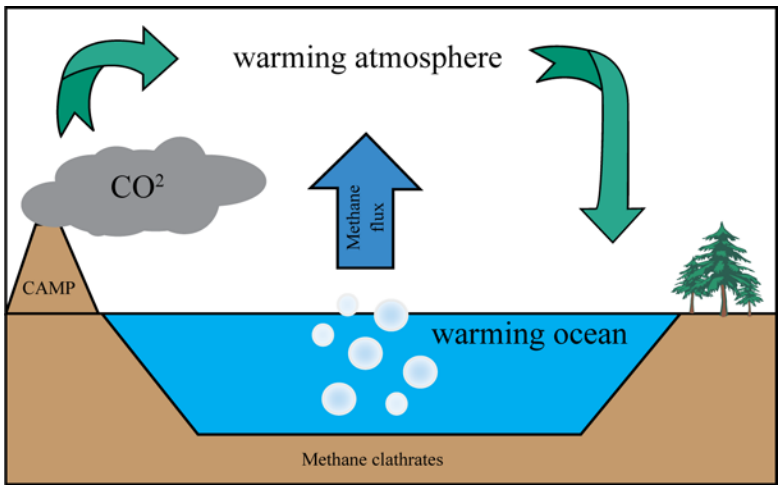

Figure 1 Model of two step climate change adapted from M. Ruhl et al., in prep. (1) warming of atmosphere and ocean due to CO_2 outgassing CAMP (2) triggering the release of methane by destabilizing the methane clathrates and causing additional warming of the atmosphere and ocean.

3 Material and Methods

3.1 Geographical and geological setting

The Kuhjoch section (47°29'02''N/11°31'50''E) is located 25 km north-north-east of Innsbruck and 5 km north-east of the village Hinterriss. The section is part of the Karwendel syncline, stretching from east to west, with a length of about 30 km. This synclinal structure lies within the Lechtal nappe of the western Northern Calcareous Alps. The section is situated in a natural reserve (Karwendel Naturpark) on a mountain ledge between Kuhjoch peak, the Holzelstaljoch peak and Ochsentaljoch peak. Detailed location maps of the section is given in A. Hillebrandt et al. (2007)

The Kuhjoch section is situated within the intra-platform Eiberg basin that developed during the late Rhaetian. This intra-platform was situated on a 300 km wide and approximately 500 km long shelf strip at the western end of the Tethys Ocean during the Rhaetian (Kürschner et al., 2007). This intra-platform was bordered to the north and south by the carbonate platforms of the Oberrhaet limestone that also formed during the Late Rhaetian (Figure 2). The southern Oberrhaet limestone bordered to an open shelf basin also called the Hallstat basin and the northern Oberrhaet limestone was bordered landward by the shallower Allgäu basin (Krystyn et al., 2005). During the deposition of the Eiberg member on top of the Hochalm member (together Koessen formation), the intra-platform Eiberg Basin deepened because of continuous subsidence during the latest Rhaetian. This had as a result that the deeper parts of the basin were not affected by the End-Triassic sea level lowering and fully marine conditions remained (A. v. Hillebrandt & Urlichs, 2008; A. v. Hillebrandt & Krystyn, 2009; Krystyn et al., 2005). But there still is a clear sedimentary turnover from full marine limestones of the Koessen formation towards more restricted shallow marine marly sediments of the Kendlbach formation.

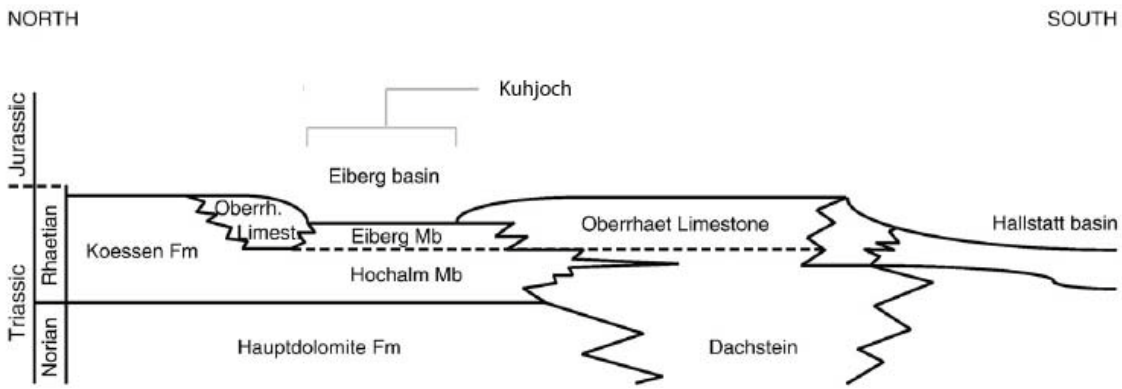

Figure 2 Geological setting of the Kuhjoch section after (adapted from Krystyn et al., 2005).

3.2 Lithostratigraphy

The main sections starts 2 meter below the top of the Koessen formation/Eiberg Member this consists of well bedded and variable thick bioturbated limestone (bioclastic wackestones) beds (up to 50 cm). The top limestone bed of the Eiberg member (20 cm) differs because it has a darker color and more platy weathering due to an increased clay content and the upper part is laminated. The upper most (1 cm) of this bed is a black and bituminous layer, with numerous bivalves and fish remains (scales), possibly indicating an anoxic event and the peak of the regression. This is the boundary between the transition from deep to more restricted shallower marine deposits.

The Kendlbach formation which succeeds the Koessen formation consists of more terrigenous marls, indicating shallow marine shelf conditions which increasingly deepen towards the top part. On top of the Koessen limestones, a layer (43 cm) of grey-brown marl is deposited, which become more yellowish, weathered and partly laminated in the upper 30 cm. These marls are in turn followed by the Schattwald beds (200 cm) comprised of red marls. These conspicuous beds have been found in multiple sections over an extended area. The Schattwald beds contain a small fault at the top part which comprises a small hiatus. Although the red color, these deposits are of marine origin, because abundant marine fauna has been found. This is then succeeded by again a thicker unit of olive grey marls with increasingly more thin silt- and sandstone layer towards the top. The transition from the Tiefengraben towards the Breitenberg member is not well exposed. A naturally well exposed outcrop of this part is found at the Ochenstaljoch (A. Hillebrandt et al., 2007; A. v. Hillebrandt & Urlichs, 2008; A. v. Hillebrandt & Krystyn, 2009; Krystyn et al., 2005; M. Ruhl et al., 2009).

The region of the Kuhjoch section underwent drastic deformation during the Alpine orogeny (e.g. the Karwendel syncline) and this created probably the fault present in the Schattwald beds. This fault is absent in a subsection located east of the main Kuhjoch section, there the C-isotope curve and palynology is continues (previous study; bachelor thesis). For the chemical analyses which included $\delta^{18}O$ and $\delta\ ^{13}C$ measurements on foraminiferal shells, a second section, the Hochalplgraben has been used. This section is located in close proximity of Kuhjoch and has an almost similar lithology, biostratigraphy and carbon-isotopestratigraphy (Figure 11 and (Bonis, Ruhl, & Kürschner, 2010a))

3.3 Biostratigraphy

The biostratigraphy of the Triassic-Jurassic boundary in the Kuhjoch section is largely based upon ammonite biozones (A. Hillebrandt et al., 2007; A. v. Hillebrandt & Krystyn, 2009). The Triassic-Jurassic Boundary Working Group determined in 2008 that the ammonite species *Psiloceras spelae* known from Nevada (USA) defines the first Jurassic ammonite biohorizon and this can then be used to define the Tr-J boundary, globally, and helps correlate deposits of the Tethys and Panthalassa paleo-oceans.

In 2007 several species of *Psiloceras spelae* were found in the Kuhjoch section but they do not show all characteristics as seen in the specimens from Nevada and they are therefore classified as a regional subspecies *Psiloceras spelae* n. spp. These specimens can still be used as guide fossils for the Tr-J boundary (A. v. Hillebrandt & Krystyn, 2009). Furthermore there has been extensive research done on the palynostratigraphy and carbon-isotopestratigraphy of the Tiefengraben section, which is another Tr-J boundary section within the Eiberg basin (Kürschner et al., 2007). In the Tiefengraben section five palynomorph assemblage zones have been described; the main features are summarized below;

Rhaetipollis-Limbosporites zone (RL zone): This zone is characterized by a low diversity assemblage with high numbers of *Classopollis meyeriana* and *Classopollis torosus* (collectively 60%) together with smaller numbers of *Ovalipollis pseudoalatus* (30%). *Rhaetipollis germanicus*, *Limbosporites lundbladii* and *Cingulizonates rhaeticus* are present.

Rhaetipollis-Porcellispora zone (RPo zone): At the base of this zone spore diversity and abundance, mainly of *Porcellispora longdonensis* and *Calamaspora tener* show a short maximum or acme. The lower part shows a brief decline in *Classopollis* (30%) and a rise in *Vitreisporites.* The middle part of the zone *Classopollis torosus* but especially *Classopollis meyeriana* reaches a maximum of 60%. The top part of the zone has a distinct decrease of *Classopollis* (20%) accompanied by a marked increase in *Polypodiisporites polymicroforatus, Calamaspora tener* and *Deltoidospora* spp.

Trachyspora- Porcellispora zone (TPo zone): This zone is characterized by a continued decline in *Classopollis meyeriana* (<10%) and *Classopollis torosus* even disappears for a short interval. Furthermore the assemblage is marked by a decrease in *Calamaspora tener*, *Polypodiisporites polymicroforatus* and *Deltoidospora* spp. and accompanied by a rise of *Carnisporites* sp. div., *Concavisporites* spp., *Porcellispora longdonensis* and *Trachysporites fuscus*. Distinctive is the total absence of *Ovalipollis pseudoalatus*.

Trachyspora- Heliosporites zone (TH zone) : The most distinct feature is the reappearance of *Classopollis torosus* while the numbers *Classopollis meyeriana* remain constant. Furthermore there is an increase upsection of *Porcellispora longdonensis*, which is followed by a peak of *Heliosporites reissingeri* (30%). *Heliosporites reissingeri* and *Porcellispora longdonensis* show a decrease again to 10% and 5% respectively in the upper part of the section. Furthermore there are some peaks of echinate and baculate trilete spores at the base of the zone. Of especially biostratigraphic importance is the first occurrence of *Cerebropollenites thiergartii* at the base of this zone.

Trachysporites-Pinuspollenites zone (TPi zone) : The main feature of this zone is the dominance of *Trachysporites* (30%) and two sharp maxima of 60%, but also the occurrence *Pinuspollenites minimus* (5-10%).

Extensive palynostratigraphic research has also been performed on the Hochalplgraben and a former low resolution research on Kuhjoch (Bonis et al., 2009). In these studies respectively 5 and 4 palynomorph assemblage zones have been described but they appear to miss a palynomorph assemblage zone. Additionally, carbon isotopic records, show a sharp shift within the onset of the main CIE when compared with the Tiefengraben section. In a subsection east of the main Kuhjoch section this palynomorph zone has been found together with a more gradual onset of the main CIE (previous study; bachelor thesis).

3.4 Palynological analysis

The dataset is based on a few samples from the lowermost part of the section previously analyzed by (Bonis, Ruhl, & Kürschner, 2010a) and 35 analyzed samples in this study. For the 35 palynological samples approximately 12 - 14 gram sediment was cleaned and crushed into fragmented smaller than 1 mm. Then the samples were dried in an oven at 60 ° C for 24 hours. A lycopodium spore tablet (contains 10679 spores in average) was added to each sample and the dry weight was measured in order to obtain quantitative data. After that cold HCL (10%) and cold HF (38%) was applied on the samples and this was repeated for a second time, this treatment will remove carbonate and silicate minerals. Subsequently the residue is washed until it reaches neutral pH and sieved with a 250 µm mesh to remove the larger particles and a 15 µm mesh to remove the finer particles. And as last step $ZnCl_2$ was added to the residue to remove the remaining minerals (e.g. pyrite). Lastly, two slides were prepared from each sample, with glycerine jelly standards according to Kürschner et al. (2007).

Relative abundances were calculated and plotted with Tillia/TilliaGraph and TGView computer programs (Grimm,1991-2001). Furthermore palynomorph assemblage zones were recognized with the help of the statistical program CONISS (Grimm, 1987).

3.5 Multivariate statistical analyses

To represent the multidimensional dataset containing the palynomorphs, Principal Component Analysis (PCA) is used. This technique helps to explain the variance within the dataset in respect with unknown environmental parameters. The analyses on the palynological data were performed by the computer program CANOCO (Ter Braak, 1996-2004), with a square root transformation of the species data, centered by variables (taxa). Species with less than 5% abundance are ignored to reduce the influence of rare taxa on the ordination. The results are then plotted as the species scores on the first and second axis. Although numerous axis can be generated, but the first and second axis explain the majority of the variance in the species variance. Finally, sample scores have been plotted alongside the depth of the samples.

3.6 Foraminifera

Benthic foraminiferal shells from the collection of Hillebrandt, A.v. (Technical University of Berlin) were used to determine oxygen- and carbon isotope composition. Specimens from the Nodosariidae family (producing calcite) and from Oberhauserellidae (producing aragonite) were selected. In total seven sampling heights were used, from these samples, six contained specimens of *Dentalina* spp. (Nodosariidae) and one sample also contained the large specimens; *Marginulinopsis* spp. additionally four samples contained *Reinholdella* spp. (Robertinina). Three samples of Hochalplgraben included Oberhauserellidae and one, Praegubkinella and/or Oberhauserella specimens.
A first order approximation of the preservational state of the specimens was based on light microscopy and allowed selection of specimens for further analysis. Further detection of recrystallization and the presence of microtextural characteristics, e.g. test walls and pore structures, were done by XL30FEG SEM in Utrecht (Figure 12).

3.6.1 Electron Microprobe

Electron microprobe –scanning electron microscopy allowed determination of the elemental composition of selected sites on the foraminifera. Elemental analyses were performed by the electron microprobe–scanning electron microscope (JEOL JXA-8600 superprobe, Noran Instruments) at the University of Utrecht. For this a slide with the foraminifera samples embedded within an alraldite resin, was prepared and secondly the slide was polished to reveal a cross section of the chambers. Eventually the exposed foraminiferal shell was carbon-coated (Figure 13).

3.6.2 Raman Spectroscopy

Further analyses of the chemical crystal lattice were performed by confocal Raman spectroscopy (alpha300 R) at the Alfred Wegener Institute. A Raman spectrum shows the energy shift of the excitation light (laser) as a result of elastic or inelastic scattering by the molecules in a sample. Therefore this is a nondestructive imaging technique which combines thousands of spectra in one picture. This way chemical properties can be analyzed with great accurate and with high a resolution (down to 200 nm). Hence the minute differences between the calcite and aragonite lattices could be detected with great precision.

3.7 Carbon and oxygen isotope analysis

Preparation for isotopic analyses was different for the two different genera. For *Reinholdella* spp., the infill was removed from the foraminifer's chambers by crushing the foraminifera between two slides and isolating the $CaCO_3$ from the infill. In contrary to Oberhauserellidae, the specimens of *Dentalina* spp. were measured without an extra cleaning step. The $\delta^{18}O$ and $\delta\ ^{13}C$ measurements were performed at the University of Utrecht , using a CARBO-KIEL automated carbonate preparation device linked online to a Finnigan MAT253b mass spectrometer. Calibration to the VPDB (Vienna Pee Dee Belemnite) is done by the international standard NBSΔ19 and in house standard Naxos with an error usually not bigger than 0.02‰ and 0.08‰.

3.8 Paleothermometry

The $\delta^{18}O$ values were used to calculate the temperature of the ambient seawater. Even though the foraminifera are benthic, the semi-restricted Eiberg basin never had a depth of more than 200 meter (A. Hillebrandt et al., 2007). Hence, the ambient seawater had similar properties as the surface ocean, for that reason the $\delta^{18}O_{water}$ is most probably affected by the evaporation/precipitation balance which depends on latitude. This offset is corrected with equation (1) of J. Zachos et al. (2001), additionally the $\delta^{18}O_{water}$ is corrected for an ice free world (-1.2%; (J. Zachos et al., 2001) because there is a low probability for continental icesheets at this time interval, inferred from modeling studies (Huynh & Poulsen, 2005). The temperatures were calculated with equation (2) of Bemis et al. (1998) for the calcite species and equation (3) Grossman & Ku (1986) for the aragonite species.

$$offset\ \delta^{18}O_{water} = 0.576 + (0.041 \times \lambda) - (0.0017 * \lambda^2) + (0.0000135 \times \lambda^3) \quad (1)$$

$$T(°C) = 16.5 - 4.81(\delta^{18}O_{carb} - \delta^{18}O_{water}) \quad (2)$$

$$T(°C) = 20.6 - 4.34(\delta^{18}O_{arg} - \delta^{18}O_{water}) \quad (3)$$

4 Results

4.1 Palynology

4.1.1 Terrestrial palynology

The terrestrial palynomorphs assemblages of the Kuhjoch section are marked by extensive changes throughout the section. This can already be observed within the pollen:spores ratio which decreases towards the top (Figure 3). At the base of the Kendlbach formation around 90 % of the terrestrial assemblage consists of pollen whereas in the Schattwald beds this decreases to only 30 %. The fraction of pollen continues to decrease even further, above the Schattwald beds, to 10% and stays constant upsection. With the exception of two peaks of more than 30%, one is situated directly above the main CIE and another one at 460 cm above the base. To obtain a better understanding of the changing palynomorph assemblages, clustering analyses was performed. This approach yielded four distinct palynomorph assemblages (KH2-5), a fifth assemblage is defined by the first large peak of *Classopollis meyeriana* (KH1) (Figure 9).

KH1

In this zone which constitutes only 28 cm of the total section (~ 2300 cm), *Classopollis meyeriana* is the dominant component with a maximum of more than 90 %. Another important component is *Ovalipollis pseudoalatus* (20%) which has a peak in the first sample. This assemblage is further characterized by several simultaneous acmes in different spore types; *Conbaculatisporites* spp. (20%) *Baculatisporites* spp. (20%),

Carnisporites anteriscus (10%), *Acanthotriletes varius* (10%), *Calamaspora tener* (10%), *Todisporites* spp. (10%) and *Riccisporites tuberculates* (10%).

KH2

This assemblage is mainly characterized by rapidly decreasing numbers of *Classopollis meyeriana*, while *Classopollis torosus* increases somewhat, to 20%. Furthermore the diversity and abundance within spores increases. The dominant spore types are *Polypodiisporites microforatus* (>20%), but also *Deltoidospora* spp., *Concavisporites* spp. and *Riccisporites tuberculates*. In addition *Vitreisporites Bjuvensis* (20%) is very abundant. Additionally the palynomorphs are exceptionally well preserved, in contrary to rest of the section. At the boundary between KH2 and KH3 there is again an acme of *Classopollis meyeriana* but smaller than the previous acme (>30%). At the top of this zone Heliosporites and Trachysporites enter the record.

KH3

After the peak, *Classopollis meyeriana* remains a more important constituent then in KH2, with values of up to 20% and at 460 cm from the base, an acme of over 30%. But other pollen that were common in previous zones are totally absent such as; *Vitreisporites Bjuvensis*, *Ovalipollis pseudoalatus* and *Rhaetipollis germanicus*. Furthermore qualitative analyses of the samples assigned the first occurrences of both the Jurassic markers *Cerebropollenites thiergartii* and *Ischyosporites variegatus* to the base of this zone. There is in addition a change in the composition of spore taxa with the almost complete disappearance of *Polypodiisporites microforatus* and a sharp increase of *Heliosporites* (10-25%) and *Trachysporites* (30%). Additionally *Riccisporites tuberculatus* is generally of low abundance but there are some acmes of up to 15%. It is also strikingly that from this height upward the palynomorphs are of poorer quality.

KH4

In this assemblage *Classopollis meyeriana* decrease to even lower numbers of around 10% and stays very constant throughout the section. There are also marked changes within the sporomorph taxa; *Trachysporites* reaches even higher abundances of more than 40% and *Riccisporites* increases at the bottom part to 20 %. While *Heliosporites* is characterized by a decline, but with some peaks reaching up to 20 %.

KH5

The most notable feature of this assemblage is the increase of *Pinuspollenites minimus*. Furthermore it is marked with an further increase of *Riccisporites tuberculatus* and a further decline of *Heliosporites*. While *Trachysporites* is still the dominant component.

4.1.2 Aquatic palynomorphs

Most of the Kuhjoch section is dominated by terrestrial palynomorphs, with aquatic palynomorphs only being a minor element (<30%). But there are some exceptions, mainly at the height just above the initial CIE there is a peak of almost 90 % and another peak just above the main shift in $\delta^{13}C_{toc}$ record, of more than 50% (Figure 3). Both maxima are accompanied by high concentrations of the aquatic palynomorphs. At the base of the section the dinoflagellate cysts of *Rhaetogonyaulax rhaetica* are a major

constituent of the marine palynomorphs . This is intersected by an acme of prasinophytes mainly presented by *Cymatiosphaera polypartie* and for a smaller part by cf. *Leiospharidia* and *Tasmanites* sp. After this acme of prasinophytes, *Rheatogonyaulax rhaetica* starts to decline while *Dapcodinium priscum* starts to increase in abundance. Also the freshwater tolerant *Botryoccocus* spp. appears for the first time. Within the Schattwald beds total numbers of aquatic palynomorphs are low. The major constituent of the aquatic palynomorphs are now prasinophytes mainly cf. *Leiospharidia* instead of dinoflagellate cysts. Above the Schattwald beds total numbers of aquatic palynomorphs increases drastically again with peaks of up to 500 counts per sample. The assemblages are from there onward mainly comprised of cf. *Leiospharidia*. Only at the top of the section dinoflagellate cysts become again a more important element. With first a peak in an unknown (Type 1) dinoflagellate cysts followed by a simultaneous peak in *Dapcodinium priscum* and *Valveodinium koessenium* (Figure 10).

4.1.3 Deformed palynomorphs

An important component of the total palynomorph assemblage are deformed palynomorphs. These are the degenerated counter parts of presumably terrestrial palynomorphs. They do not have the microtextural marks as normal pollen and spores would have (although some have a trilete mark) but they resemble them in size and shape (round, oval, triangular). The most convincing evidence that these deformed palynomorphs once were pollen and spores are tetraethers, with some pristine specimens and deformed specimens still attached to each other (see plate 5). In the first 2 meters of the section deformed palynomorphs are rare. Above this level there is a sudden increase to 50 % of the total terrestrial palynomorphs. In the upper part of the section the deformed palynomorphs are consistently an important factor of the terrestrial palynomorphs, with some peaks reaching up to 80 % (Figure 3).

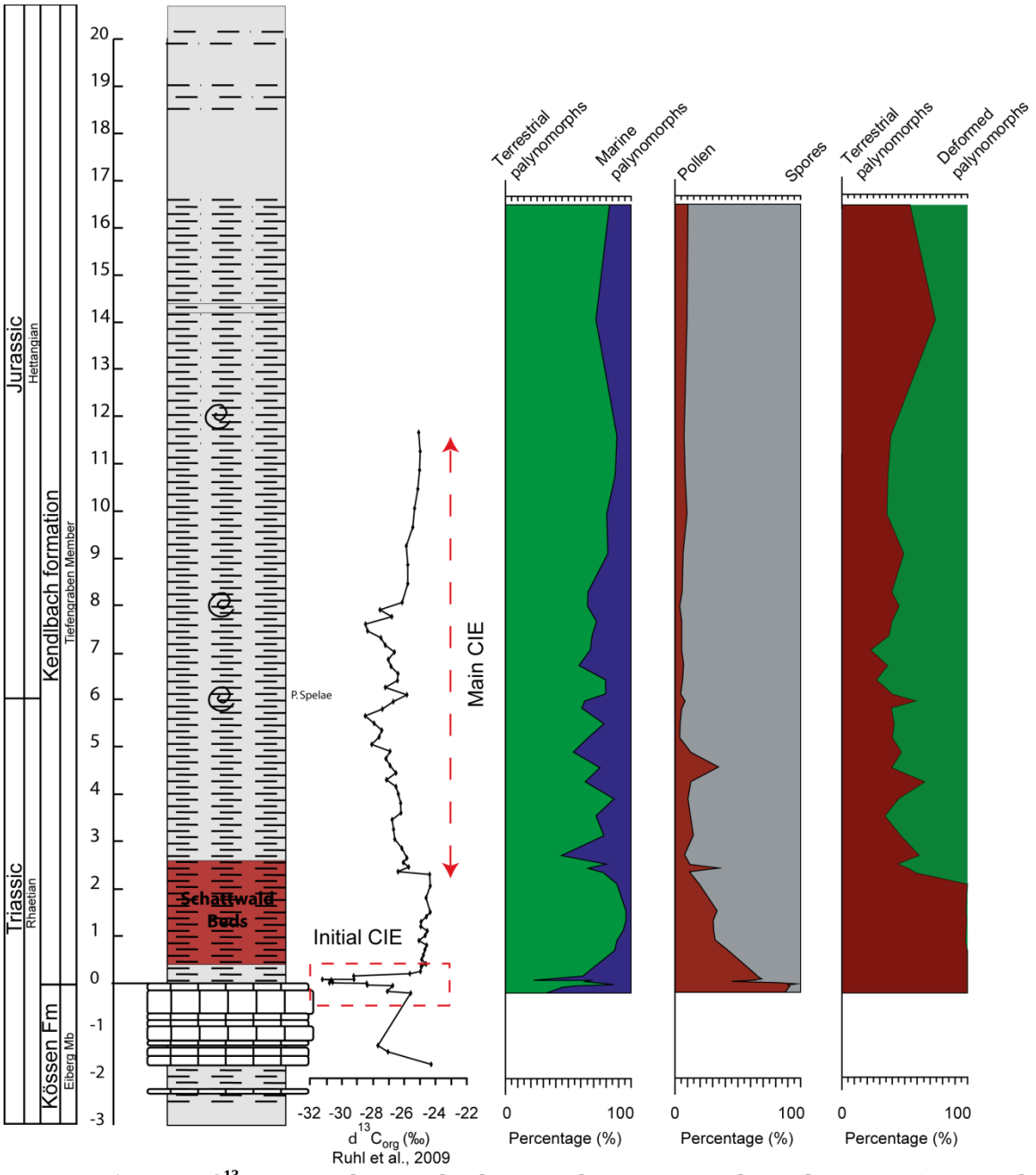

Figure 3 Lithology, $\delta^{13}C_{org}$ record, general palynomorph composition denoted in ratios (terrestrial: marine palynomorphs, pollen: spores and terrestrial: deformed palynomorphs).

4.2 Multivariate statistical analyses

The first PCA axis from Kuhjoch explains 48.5 % of the total variance within the terrestrial palynomorph dataset. The majority of spores, scores negative on this axis while all pollen species (except *Pinuspollenites minimus*) score positive. With *Trachysporites fuscus* and *Heliosporites reissingeri* most prominently at the negative end, and *Classopollis Meyeriana*, *Classopollis Torosus*, *Vitreisporites Bjuvensis* and *Polypodiisporites microforatus* at the positive end. The second PCA axis explains an

additional 14.3 % of the total variance within the terrestrial palynomorph dataset. The most positive scores on this axis are *Polypodiisporites microforatus*, *Pinuspollenites minimus*, *Vitreisporites Bjuvensis* and several *Carnisporites* species. Especially *Classopollis Meyeriana* has a high species score on the positive side of this axis (Figure 4). Additionally the sample scores of both axis have been plotted against depth (Figure 14). The sample scores of the first axis start out positive, except for a small peak at the base of the section. At 230 cm above the base there is a shift to negative values, which persist until the top of the section. The sample scores of the second axis, have the most positive value at the base of the section, after this peak sample scores become rapidly negative. Until 230 cm above the base were the sample scores become again positive.

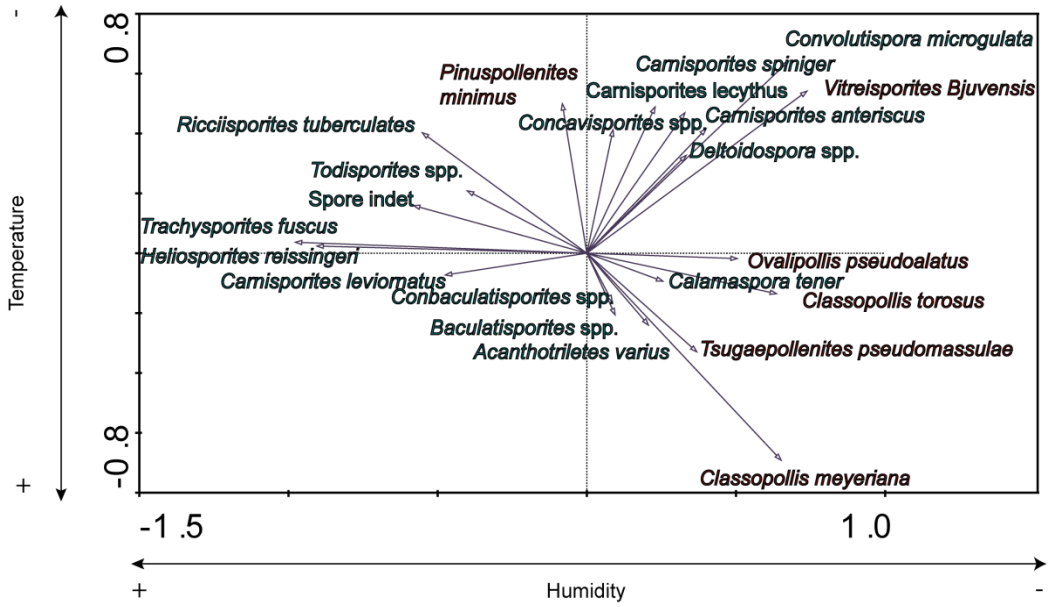

Figure 4 Principal Component Analysis ordination plot of the palynomorph dataset of Kuhjoch.

4.3 Foraminifera

4.3.1 Microstructural preservation

Scanning Electron Microscopy revealed that the surface of most specimens were not smooth as would be expected from there well-preserved appearance under the light microscope. Relatively coarse surface textures may well have resulted from partial dissolution and remineralization. Although aragonite is the less stable $CaCO_3$-polymorph, *Reinholdella spp.*, *Praegubkinella spp.* and *Oberhauserella spp.* appear better preserved then the Nodosariidae. Some of these specimens contained a number of microtextural structures (e.g. pores) indicating that recrystallization has only partially altered the original morphology of the foraminiferal calcite (Figure 5).

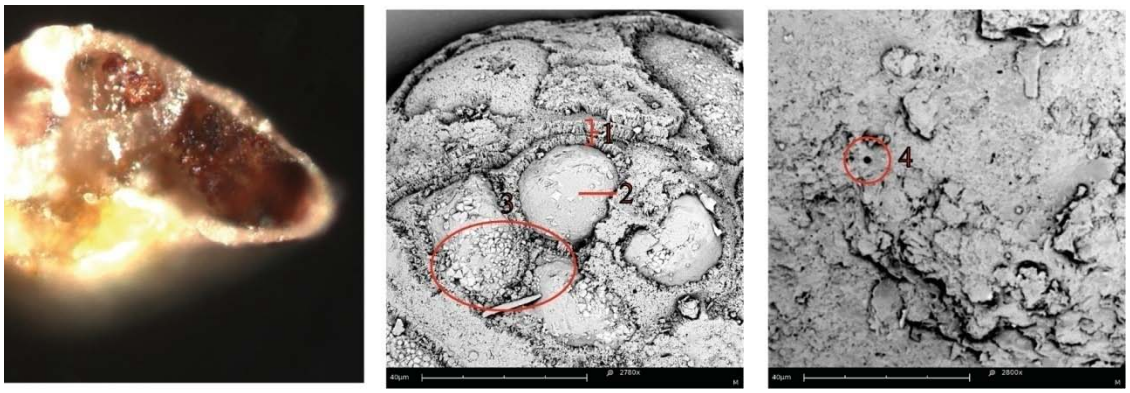

Figure 5 Left; cross section of *Reinholdella* spp., showing the white CaCO3 and chamber infill (red). middle and right; SEM images of *Reinholdella* spp. (1) test wall (2) infill of chamber (3) crystallites (4) pore structure.

4.3.2 Elemental analyses

Due to their well preservation, elemental analysis was performed on selected specimens from the Oberhauserellidae. The electron microprobe-electron microscopy determined that the chamber walls contain Ca but also smaller amounts of Mg and Sr (Figure 13). The presence of rare earth elements like Te, W and Re are probably the result of uncertainties inherent with the method used and contaminations e.g. Tungsten (W) is part of the polishing agent used for the preparation of the slide. The infill consists of Al, Si and Ca, furthermore the crystallites (Figure 5.3) covering parts of the specimens, contain Fe and S, resembling pyrite and iron oxides (Figure 7; Figure 13) . Raman spectroscopy additionally revealed that the $CaCO_3$-phase of several specimens of *Reinholdella* spp. partly consisted of aragonite.

4.4 Carbon and oxygen isotopes

The $\delta^{18}O$ o f $\delta^{13}C_{carb}$ of *Reinholdella* spp. specimens of the Kuhjoch and Hochalplgraben section were respectively; -1.93 and -2.18 ‰ for $\delta^{18}O$ and 1.95 and 1.11 ‰ for $\delta^{13}C_{carb}$ (Figure 9). The $\delta^{18}O$ and $\delta^{13}C_{carb}$ of *Dentalina* spp. covered a more extended interval (Figure 9). With the lowest values $\delta^{18}O$ at the base (-3.72 to -3.16 ‰), more positive $\delta^{18}O$ values for the two subsequent sampling heights, above the Schattwald beds (-2.56 to -2.35, -3.11 to -2.77 ‰) and for the two samples located in the upper part of the section, the spread between the $\delta^{18}O$ measurements are higher (-3.17 to -2.26, -3.19 to -2.36 ‰). The $\delta^{13}C_{carb}$ values yielded a similar pattern with lowest values at the base -0.49 to 0.22 ‰, and higher values upsection, subsequently; 0.40 to 0.69, 0.09 to 0.37, 0.60 to 1.03 and 1.11 to 1.75 ‰. Additionally measurements on *Margunilopsis* spp. yielded values ranging from -0.91 to -0.46 ‰ for $\delta^{13}C_{carb}$ and -1.66 to -0.86 ‰ for $\delta^{18}O$. The relation between $\delta^{13}C_{carb}$ and $\delta^{18}O$ is species-specific and potentially reveals different levels of diagenetically altered $CaCO_3$ (Figure 6).

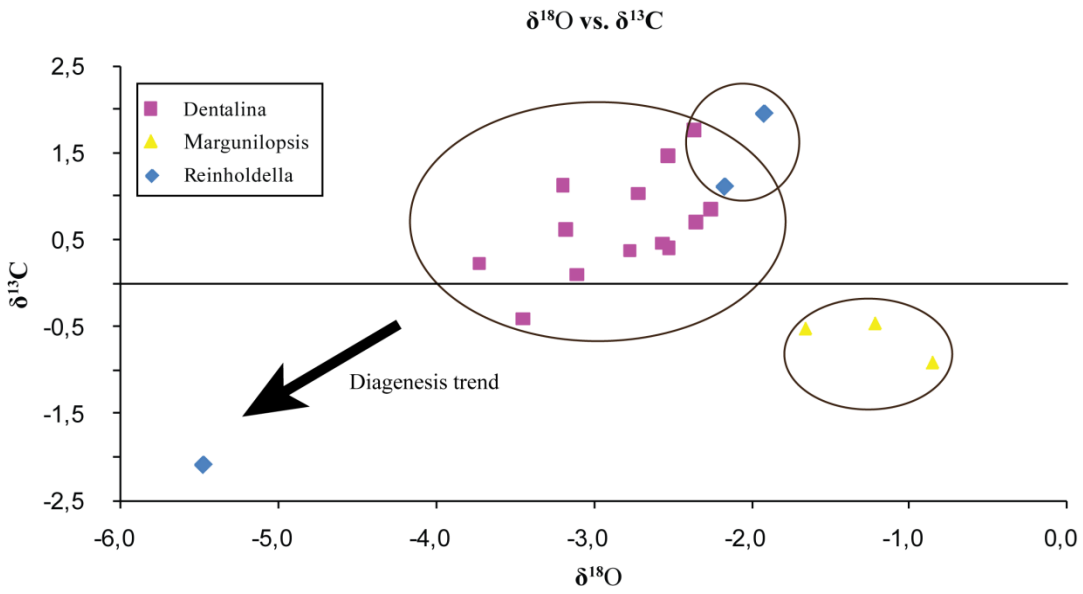

Figure 6 $\delta^{13}C_{carb}$ and $\delta^{18}O$ from three genera of foraminifera from the Kuhjoch section. Values towards the lower left corner indicate more diagenetically altered $CaCO_3$.

The highest temperatures (30 to 33°C) inferred from $\delta^{18}O$, are found at the base of the section and somewhat colder temperatures (25.5 to 27.5°C) directly above the Schattwald beds. After that temperatures first increase (27.5 to 29°C). The temperatures at the top of the section cover a wider range due to the larger spread between $\delta^{18}O$ data points (26 to 29°C followed by 25.5 to 29°C) (Figure 14).

5 Discussion

5.1 Palynology

5.1.1 Terrestrial palynology

Five palynomorph assemblages have been established in this detailed study of Kuhjoch. The KH 1 assemblage is similar to the most upper part of the RL zone, because it is marked by a large peak of *Classopollis meyeriana* (>90%), which has also been observed in Hochalplgraben. Additionally the high abundances of *Ovalipollis pseudoalatus*, *Conbaculatisporites* spp. and *Baculatisporites* spp. are also similar as in Hochalplgraben. Given the lower abundance of *Classopollis meyeriana* and the increase of *Vitreisporites* and *Polypodiisporites polymicroforatus* this assemblage probably resembles the RPo zone of the Tiefengraben. Because of the sharp increase of *Heliosporites reissingeri* and *Trachysporites fuscus* and the total absence of *Polypodiisporites polymicroforatus* and *Vitreisporites* the next zone is most probably the TH zone. Similarly as in the Hochalplgraben section the next assemblage also belongs to the TH zone and resembles the H4a zone of Hochalplgraben with the decrease of *Heliosporites reissingeri* and an increase of *Riccisporites tuberculatus*. The Last assemblage resembles the TPi zone of Tiefengraben, with the increase of *Pinuspollenites minimus.*

Previous studies in the Northern Calcareous Alps (Morbey, 1975; Schuurman, 1979) could distinguish several distinct terrestrial palynomorph assemblages. This research gave a more detailed representation of the micro-floral record across the T-J boundary together with carbon-isotope stratigraphy, which resembles a previous detailed study of Tiefengraben (Kürschner et al., 2007). Additionally this site has the ammonite *P. Spelae* n. spp., which marks the base of the Jurassic. At a previous study by Bonis et al. (2009) on Kuhjoch and Hochalplgraben, small differences in the palynomorph zones were observed probably due to differences in sampling resolution. With this new detailed study of Kuhjoch it was possible to resolve these differences and ensures an even better correlation between sites of the Eiberg basin (Figure 11).

5.1.2 Vegetation changes and climate

The terrestrial palynomorph assemblage are not only used as a tool for stratigraphic correlation, it is furthermore useful as a tool to reconstruct the composition of the vegetation, which in turn could reflect environmental and/or climatic factors controlling this composition. To better understand and interpret the data, multivariate statistical analyses have been performed.

On the first axis all but one pollen producing taxa scored positive (Figure 4). The most studied of the pollen taxa is *Classopollis meyeriana* which is produced by Cheirolepiaceous conifers and has often been associated with arid conditions. During global aridification events in the Late Jurassic to the Early Cretaceous, *Classopollis* becomes dominant or even mono-dominant species on the southern parts of the Eurasian continent, while moisture loving plant groups are decimated and migrate northward (Vakhrameev, 1987). Furthermore *Classopollis* has often been found in association with evaporitic deposits (Vakhrameev, 1981 cited by Hallam et al., 1993)

On the opposite side of the first axis there are mainly spore producing species (e.g. ferns, liverworts and horsetails) and these are indicative of more humid conditions (Bonis & Kürschner, in prep. a). Together with *Pinuspollenites minimus* which belongs to an ancient Pinacaea, that probably required a high degree of moisture. Since this plant species retreated northward to more humid and temperate climates during periods of drought in the Late Jurassic (Vakhrameev, 1987).

The second PCA axis explains 14.3 % of the total variance within the dataset, so it is less pronounced. And its relation with an environmental/climatic parameter is somewhat more obscure (Figure 4). Except that *Classopollis meyeriana* scores exceptionally negative on the second PCA axis and this can again be assigned to the dominance of these species during warm and dry periods. Hence this axis probably reflects a gradient from colder to warmer climate conditions. *Classopollis torosus* has been reported to occur at higher latitude and is therefore assumed to be more cold adapted. A clear separation between these two *Classopollis* species as in previous studies (Bonis et al., 2009) is absent, however *Classopollis torosus* plots somewhat less negative in this PCA plot. The *Vitreisporites bjuvensis* is produced by a seedfern and has a more pronounced positive score on the second PCA axis. Since this taxon is abundant at higher paleolatitudes e.g. Greenland sections (Pedersen & Lund, 1980), this is additional evidence that the second axis represent cold versus warm conditions. Together with *Pinuspollenites minimus* which has been reported to occur at the more temperate northern climates associated with Late Jurassic drought events (Vakhrameev, 1987). For a full list

of the botanical affinities of the different palynomorphs see Bonis & Kürschner, in prep. a.

It is possible to extrapolate these inferred climatic gradients of the PCA axis to the sample scores and give an interpretation of the changing palynomorph assemblages throughout the section. The micro-floral record from the base of the Kendlbach formation, reflect major changes in the paleoenvironment, especially in the second PCA axis. There is an acme within Cheirolepiaceous conifers which are associated with warm and dry conditions this then abruptly changes to vegetation dominated by more cold adapted seedferns. This translates into a warm event coinciding with the initial CIE. (Figure 14). After this short warm event, an abrupt shift to relatively cooler and dryer climate occurs. Similarly as observed by Korte et al. (2009), in a $\delta^{18}O$ record of biogenic calciumcarbonate. Following that, the climate becomes increasingly more humid, which is reflected in the more abundant and diverse spore producing plant communities and this corresponds with more positive values of the $\delta^{13}C_{toc}$ record. The second major turnover in the paleoenvironement, occurs at the top part of the Schattwald beds with again a sharp peak of Cheirolepiaceous conifers, but less pronounced than the previous one. This translates into a second warming and also a short aridification pulse (Figure 14). After this the climate becomes more constant with continuously warm and humid conditions which is reflected in the dominance of spore producing plants. At 800 cm from the base there is an increase of pollen produced by ancient Pinaceae which is an indication of somewhat colder conditions as can be seen in the second PCA axis, accompanied by somewhat more positive values of $\delta^{13}C$ record (Figure 14).

5.1.3 Aquatic palynology

The change in the dominance from the dinoflagellate cysts; *Rhaetogonyaulax rhaetica* to *Dapcodinium priscum* at the transition from the Koessen formation to the Kendlbach formation has been attributed to the regression of the latest Triassic. Since *Rhaetogonyaulax rhaetica* is more adapted to open marine conditions and probably lived at greater water depth, because it has been found in low energy sediments (bay deposits). While *Dapcodinium priscum* has been found in sediments which reflect high to low energy sediments (respectively restricted bay sediments to near shore sediments) (Bonis et al., 2009 and references therein) This sea-level lowstand has also been inferred from lithological changes and the lack of deep water ammonites (A. Hillebrandt et al., 2007; A. v. Hillebrandt & Urlichs, 2008; Krystyn et al., 2005).

The acme of *Cymatiospheara polypartie* together with increased absolute counts of aquatic palynomorphs (more than 1000 count for one sample) is one of the most prominent features of this section. This feature has also been recorded in the Hochalplgraben section and as a double peak in the Tiefengraben section, in both instances, concurrent with the initial CIE. Additionally there is a sharp increase of another prasinophyte species cf. *Leiospharidia* (>60 %) higher up in the section, again accompanied by high absolute numbers. It has previously been suggested that this second peak has to do with a transgression occurring higher up in Kuhjoch (Bonis et al., 2009). While there is a deepening of the basin inferred from lithology, it is a slow long-term sea-level rise which culminates in a sea-level highstand only late in the Sinemurian (Krystyn et al., 2005). However the numbers of cf. *Leiospharidia* suddenly decrease at the top part of Kuhjoch and *Dapcodinium priscum* even reappears, which would be indicative of

shallower water depths as mentioned previously. An alternative scenario is that both prasinophyte peaks indicate changing environmental circumstances. From aquatic palynomorph records of the Mesozoïcum it appears that prasinophytes are rare in general but are often more abundant when other phytoplankton is absent (Tappan, 1980). Furthermore within the Eiberg basin, high abundances of prasinophytes concur with low abundances of foraminiferal test linings (Bonis et al., 2009; Kürschner et al., 2007). Possibly because prasinophytes are sensitive to grazing of foraminifera (Metaxas & Scheibling, 1996), it has therefore been suggested that the low abundance of foraminiferal test lining and the impoverished fauna of foraminifera (A. v. Hillebrandt & Urlichs, 2008) could be an explanation for the high abundances of prasinophytes (Bonis, Ruhl, & Kürschner, 2010a)

Anoxia could be the source for this environmental stress, which could cause the destruction of the foraminiferal fauna and possibly all other oxygen dependent organisms, thereby given an advantage to prasinophytes. Such anoxia would likely be caused by stratification of the water column as a result of a fresh water lens on top of the watercolumn (Bonis, Ruhl, & Kürschner, 2010a). The mechanism for this fresh water lens could have been increased runoff due to increased seasonal precipitation (Figure 8). This is furthermore approved by the occurrence of the freshwater species *Botryococcus* spp., the absence of dinoflagellate cysts and foraminifera species indicative of hyposalinity (A. v. Hillebrandt & Urlichs, 2008). Finally, the abundance of prasinophytes in general has been associated with brackish conditions and increased nutrient availability (Bonis, Ruhl, & Kürschner, 2010a and references therein; Prauss & Riegel, 1989; Tyson, 1995). Similar events extent even beyond the Eiberg basin, as a bloom of prasinophytes has been reported to occur simultaneous with onset of the main CIE in the st.Audries bay section (UK) (Schootbrugge et al., 2007) and in the Csővár basin (Hungary) were there is an acme of prasinophytes concurrent with an negative CIE during the Late Triassic (Götz et al., 2009). It has furthermore been proposed that these prasinophyte species are 'disaster species' that survived the End-Triassic marine extinction event and flourished due to absence of other competitors and consumers. Schootbrugge et al. (2007) even suggested that these green algal phytoplankton acmes may be indicative of elevated carbon dioxide levels and widespread anoxia in shallow marine settings. This could also be an explanation for the major extinction event of marine organisms (Hallam, 2002; Raup & Sepkoski, 1982; Sepkoski, 1982).

5.2 C and O isotopes foraminiferal shells

Stable oxygen and carbon isotopes of foraminiferal calciumcarbonate are widely used tools to infer past seawater temperatures (Bice et al., 2006; Forster et al., 2007; J. C. Zachos et al., 2006; J. Zachos et al., 2001), ice volumes (Imbrie et al., 1984; Pisias et al., 1984) and seawater circulation (Fairbanks et al., 1982; Weis et al., 1988). While stable oxygen isotopes are incorporated near equilibrium when compared to seawater isotopic composition, foraminiferal $\delta^{18}O$, but particularly $\delta^{13}C_{carb}$, are known to be influenced by habitat and physiological effects (Grossman, 1987; Rohling & Cooke, 2003). On long timescales, however, the effects of large-scale climate variations (on $\delta^{18}O$) and the burial and re-oxidation of organic matter, bioproductivity and tectonic activity (on $\delta^{13}C_{carb}$) will be reflected in the biogenic $CaCO_3$ (Korte et al., 2009). To minimize the impact of

diagenetic alterations on the foraminiferal $\delta^{13}C_{carb}$ and $\delta^{18}O$, optical inspection and chemical analyses have been used to screen for diagenetic overprints. Presence of microstructures (ornamentation, pores), elemental composition and preservation of aragonite suggest that the calciumcarbonate has underwent minor chemical alterations. Aragonite is thermodynamically less stable than calcite, hence, the high Mg-calcite secreting Nodosariidae are possibly also well preserved.

The foraminiferal $\delta^{13}C_{carb}$ and $\delta^{18}O$ values form three distinct clusters for the *Reinholdella* (n=2), *Dentalina* (n=13) and *Margunilopsis* (n=3) species, despite the fact that some specimens are from the same stratigraphic height. This suggests a minor impact of chemical alteration of the $CaCO_3$ and enhances the reliability of the obtained isotopic values. The Nodosariidae specimens display an intra-species variability in $\delta^{18}O$ and $\delta^{13}C_{carb}$ of less than 1 ‰. In comparison with the cross-plot of Korte et al. (2009) diagenetically altered oyster $CaCO_3$ and whole rock samples have more negative values than those of our foraminifera, with the exception of one *Reinholdella*–specimen (Figure 6).

The first sampling height, has the lowest values of all the $\delta^{13}C_{carb}$ and $\delta^{18}O$ measurements and as expected the highest seawater temperatures, which corresponds to the upper half of the initial CIE. The samples above the onset of the main CIE are less negative for both $\delta^{13}C_{carb}$ and $\delta^{18}O$, which indicates lower seawater temperatures. With the upper two samples even more positive, especially for $\delta^{13}C_{carb}$, although the spread between data points is somewhat bigger. These values respectively correspond with more positive values within $\delta^{13}C_{toc}$.

From this small dataset it seems that similar scenarios of increased greenhouse emissions (e.g. methane injection, CO_2 outgassing volcanism or subsurface combustion of organic rich strata) and subsequent warming, can explain the existence of the initial, main CIE and possibly other secondary excursions, as $\delta^{18}O$ and $\delta^{13}C_{carb}$ superficially follow the $\delta^{13}C_{toc}$ record (Figure 14). Although the amplitudes of the $\delta^{13}C_{carb}$ record excursions are half the size of the excursions within $\delta^{13}C$ of bulk organic matter and *n*-alkanes (Figure 14). This can be explained by the fact that foraminifera are not directly found at peak negative $\delta^{13}C_{toc}$ probably due to dissolution or ecological exclusions of foraminifera (McCarren et al., 2008; Thomas, 2007). The offset between $\delta^{13}C$ of terrestrial (*n*-alkanes record) and marine (carbonate) realm during the PETM are presumed to result from e.g. soil cycling rates, relative humidity and vegetation (Bowen et al., 2004) and differences in vital effects resulting in different fractionation pathways (Schouten et al., 2007). Noticeably this difference in amplitude of carbon isotope excursions between organic matter and carbonates has often been reported for other carbon isotope anomalies of the Mesozoic (Arthur et al., 1988; Hesselbo et al., 2002; Hesselbo et al., 2007) and Cenozoïcum (Pagani et al., 2006).

It seems that the calculated temperatures are realistic when compared with other low latitude records of periods with profound carbon isotopic excursions, such as the Cretaceous black shale's (Bice et al., 2006; Schouten et al., 2003; Spicer et al., 1993) and the PETM (J. C. Zachos et al., 2006), which are supposedly periods of elevated atmospheric CO_2. The results for stable isotopes within biogenic calciumcarbonate seem promising and an extended record would be of great value for the study of extreme climate change associated with major extinction events at the End-Triassic. But other environmental parameters (e.g. the precipitation/evaporation balance) could also have

influenced $\delta^{18}O$ values and should be considered. Additional studies with independent proxies (e.g. organic proxies) could be helpful to resolve these issues.

5.3 Anoxia and framboidal pyrite

The electron microprobe revealed the presence of pyrite within the shells of some of the foraminifera (Figure 7). Additionally a large part of the palynomorph assemblage seems to be deformed (Figure 3; Figure 14), these structures are known as pyrite relic structures (Neves & Sullivan, 1964) (plate 5). Such pyrite relic structures have been found on fossil palynomorphs (Srivastava et al., 1999; Tiwari et al., 1990) and recent palynomorphs (Love & Murray, 1963). These deformations result from the growth of pyrite crystals within the exine of the palynomorph, although the pyrite itself is often removed by the palynological treatment process and only the indentations remain. These scars might have rounded or polygonal shapes, but the crystals follow the major structural elements of the palynomorphs. Neves & Sullivan (1964) divided the pyrite relic structures into three groups, polygonal, faviform and cribrate. The palynomorphs of the present study belong to the cribrate cavities (when compared with plate 2; fig 3,7,8,10,11, Neves & Sullivan, 1964). These cavities are formed by framboidal pyrite, which is similar to the pyrite associated with the foraminifera of this section.

The morphology of these pyrite crystals is an important aspect. In marine sediments there are two main crystal morphologies of pyrite; micron sized euhedral crystals and micron-sized crystals, configured as a raspberry (framboidal pyrite). Pyrite formation is a redox dependent process, since the crystal depends on a constant supply of the necessary reactants at the oxic-anoxic interface. Dissolved sulfide is produced during the bacterially mediated reduction of dissolved sulfate under anoxic conditions. Ferrous iron is produced by diffusion of Fe from the sediment (Wilkin et al., 1996). The cause for the deviation in morphology and the close association with organic matter or their fossil remains can be explained by the study of Passier et al. (1997) on sapropel S1 of the Mediterranean. Within the sapropel, framboidal pyrite is abundant and almost always found within shells of foraminifera, whereas pyrite below the sapropel consists of euhedral crystals and clusters of euhedral crystals, which are not always associated with foraminifera shells. Under anoxic conditions the simultaneous release of sulphides from insitu sulphate reduction (e.g. in the shell of the foraminifera) and dissolved Fe^{2+} from iron oxide reduction results in the rapid formation of pyrite. This fast precipitation causes a rather unorganized structure: framboidal pyrite. In contrast, when one of the two needed components relies on diffusion, slow growth of pyrite forms euhedral crystals. For example below sapropel S1 were sulphite first had to diffuse downward and pyrite growth is not at the site of the organic matter degradation. From the research of Passier et al. (1997) it can be concluded that framboidal pyrite is associated with anaerobic conditions during early diagenesis. Furthermore Wilkin et al. (1996) proposed that the size distribution of framboids are indicative of the oxygenation of the watercolumn, with smaller framboids found in sediments underlying an euxinic watercolumn and larger framboids found in sediments with an dysoxic or oxic watercolumn. Hence, framboid size distribution may be a useful paleoenvironmental indicator for the oxygen content of the overlying water column.

Concluding it may not be possible to assign the framboidal pyrite of the foraminifera species and the pyrite relic structures of palynomorphs from Kuhjoch, directly to an anoxic watercolumn. However the sudden increase and the dominance of these deformed palynomorphs in the upper part of the Kuhjoch section can certainly be ascribed to changing environmental conditions (Figure 14), where bacterial mediated sulphate reduction became suddenly much more important than before.

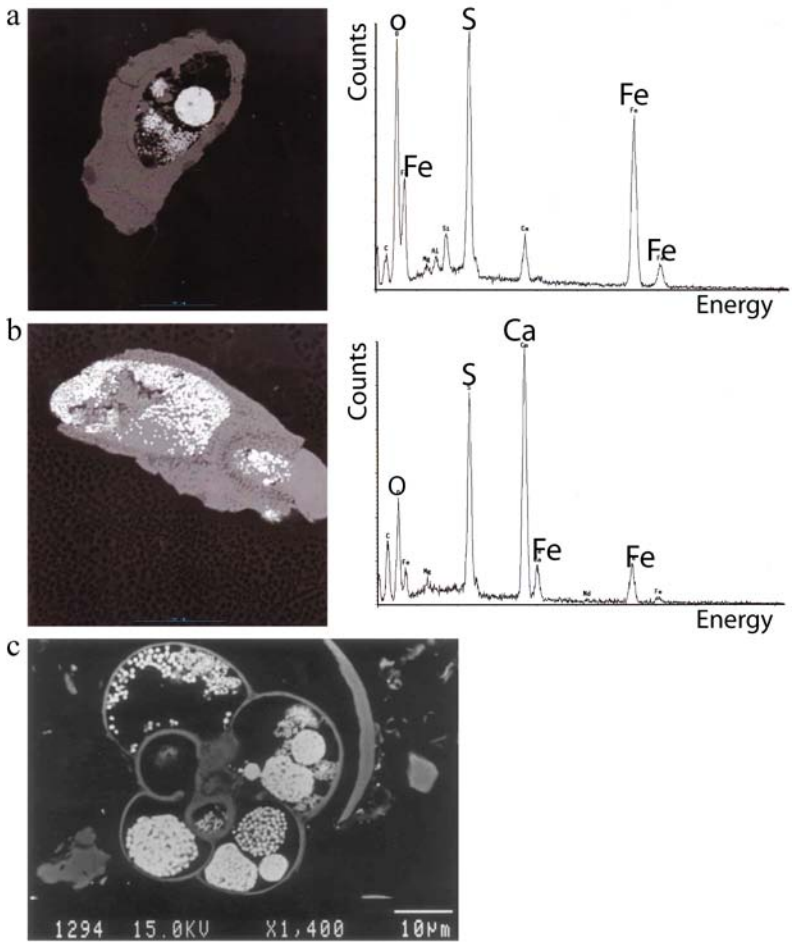

Figure 7 (a) *Reinholdella* spp. from Kuhjoch with framboidal pyrite (b) *Reinholdella* spp. from Hochalplgraben with framboidal pyrite (c) specimen from Passier et al. (1997) with framboidal within the shell of foraminifera, found in sapropel S1 of the Mediterranean.

5.4 Paleoenvironmental and climate change at the T-J boundary interval

When stacking all the data of both, the chemical analyses on the foraminifera and the palynomorph record of Kuhjoch, a detailed representation of the environmental and climatic changes of around the Tr-J boundary interval arises. The following section gives a chronological overview of the environmental and climatic changes at this site.

Statistical analyses on palynomorphs by Bonis & Kürschner (in prep. a), and this study reveal a subsequent warming and increase in humidity of the terrestrial realm at the initial CIE which is presumably caused by a methane injection. The large flux of *Classopollis meyeriana* plus increased TOC can be explained by an abrupt increase of

seasonality (humidity) within the formerly semi-arid region (Bonis, Ruhl, & Kürschner, 2010a). Causing high TOC and C*lassopollis* bearing soils to be washed in the basin. This resulted in a fresh water lens within the semi-restricted Eiberg basin, which stratified the water-column and thereby creating anoxia (Figure 8). This is supported by the occurrence of a basin wide acme of *Cymatiosphaere polypartie* because prasinophytes are known to prefer brackish to fresh water and increased nutrient contents (Bonis, Ruhl, & Kürschner, 2010a; Prauss & Riegel, 1989). Additionally low values of $\delta^{18}O$ could either; or both; be caused by increased $\delta^{18}O$ depleted runoff to the basin and a warming of the ambient seawater (*C and O isotopes foraminiferal shells*). Lastly prasinophytes could have had an advantage over other competing organisms; due to the absence of e.g. calcareous nannofossils (Schootbrugge et al., 2007), or due to decreased grazing of foraminifera, which both could have been caused by a calcification crisis, created by high pCO_2, or anoxia (Bonis, Ruhl, & Kürschner, 2010a; Hautmann, 2004; Hautmann et al., 2008).

This period is followed by a cooler and relatively dry period inferred from multivariate statistical analyses on terrestrial palynomorphs (Figure 14). Although prasinophytes abundance is still high, the concentration of marine palynomorphs is low. Additionally, dinoflagellate cysts possibly indicate more suitable environmental conditions e.g. more oxygenated water-column. Korte et al. (2009) also observed a cool period prior to the main CIE, from a $\delta^{18}O$ record of oysters at Lavernock Point (UK).

The next major environmental changes within Kuhjoch coincides with the less extreme main CIE, it is much less known if this is also a real C-cycle perturbation. There is also no evidence that this CIE concurs with an eruption pulse of CAMP (Deenen et al., 2010). But the changes in the palynomorph records are remarkably similar then with the initial CIE and elevated greenhouse gas concentrations could again be responsible for the observed warming event. Multivariate statistical analyses indicate an increase of humidity preceding the main CIE and simultaneously with the onset of the main CIE there is an abrupt warming and aridification pulse. Also $\delta^{18}O$ indicates warm ambient seawater but less warm then during the initial CIE. The onset of the main CIE is furthermore again accompanied with an pulse of *Classopollis meyeriana* followed by an increased concentration of aquatic palynomorphs, mainly dominated by the prasinophyte species cf. *Leiospharidia*. Again anoxic conditions occur, due to increased runoff during the more humid climate (Figure 8). Further evidence is the appearance of framboidal pyrite on palynomorphs and foraminifera. This implicates that anaerobic sulphate reduction by certain bacteria became suddenly more important. Again Korte et al. (2009) inferred a warming from $\delta^{18}O$ analyses on oysters and Schootbrugge et al. (2007) reported mass occurrences cf. *Leiospharidia*, coinciding with the Main CIE, suggesting warm and possibly anoxic conditions of the watercolumn at the UK sections.

Towards the top of the Kuhjoch section, carbon isotopes of both TOC and carbonate of foraminifera become again more positive. Although the spread in $\delta^{18}O$ data points is relatively large, they seem to decline somewhat (Figure 14), possibly indicating cooler ambient seawater temperatures or a decrease in $\delta^{18}O$ depleted runoff. Furthermore the increase of Pinaceae has been associated with a cooler terrestrial climate. Additionally the high abundance of prasinophytes decreases and dinoflagellate cysts become again more abundant possibly indicating more oxygenation of the water-column.

Concluding it seems that the changes in $\delta^{13}C$ are closely followed by climatic and environmental changes. Period of higher temperatures are accompanied by more humid

conditions, probably because of the thermal contrast between the continent and the sea causing enhanced monsoon systems (Figure 8), similar as observed in palynomorph record of Hochalplgraben (Bonis & Kürschner, in prep. a; Bonis & Kürschner, in prep. b)

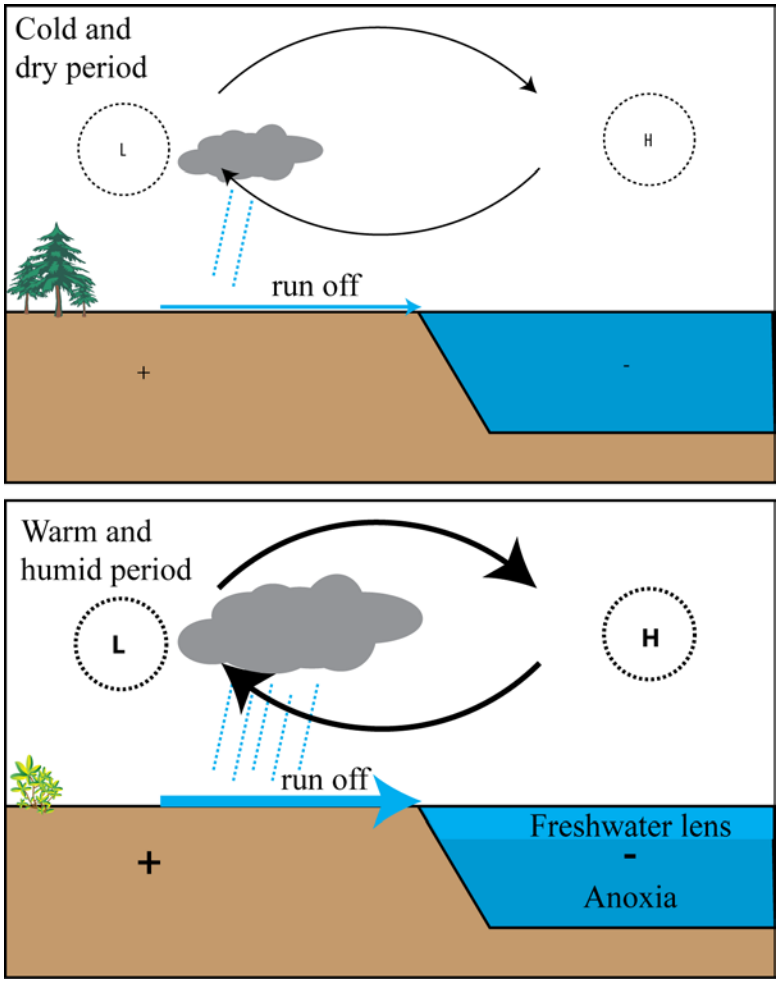

Figure 8 Climate induced variability in monsoonal strength. Top figure weak monsoon during cooler period with less thermal contrast between land and sea and a weak low pressure cell (L) develops over land, Bottom figure strong monsoon during warmer period induced by stronger thermal contrast between land and sea and a strong low pressure cell develops over land, thereby creating more runoff and a freshwater layer on the Eiberg basin with as a result anoxia of the watercolumn (Bonis, Ruhl, & Kürschner, 2010a).

5 Conclusions

Both paleoecological and geochemical data have been used for this research which dealt with climatic and paleoenvironmental changes around the Tr-J boundary. A detailed palynomorph record of the Triassic-Jurassic GSSP (Kuhjoch) has been constructed, thereby enhancing the correlation between Tr-J boundary sections of the Eiberg basin. Multivariate statistical analyses on terrestrial palynomorph assemblages together with stable O and C isotopes analyses on foraminiferal shells imply that both CIE's of latest Triassic are accompanied by warmer and more humid conditions. The increase of humid conditions resulted in an increase of precipitation leading to enhanced

runoff in the Eiberg basin. In turn causing increased nutrient content, lower salinity and anoxia of the Eiberg basin, advantageous for prasinophyte species thereby instigating large algal blooms, these conditions were unfavorable for other respiring organisms, possibly causing the marine extinctions. Framboidal pyrite crystals occurring within foraminifera shells and as relic structures on terrestrial palynomorphs are additional signs of possibly anoxic conditions within the Eiberg basin during the main CIE.

Concluding it seems that the excursions within stable C isotopes are real C-cycle perturbations which would have profound effect on the climate, paleoenvironment and possibly life in general. Massive releases of carbon from marine methane clatherates as the only source for generating these perturbations seem not feasible when compared with the modern hydrate reservoir. The assumptions based on the palynomorph and geochemical record are still debatable but the good agreement between both the records seem promising. Future research combining paleoecological and geochemical proxy records can give new insides in these periods of profound climate change.

Acknowledgements

I would like to thank my supervisors Dr. Wolfram Kürschner and Dr. Gert-Jan Reichart for support, suggestions, and providing me the opportunity to do this research. Furthermore I especially like to thank Prof. Axel von Hillebrandt for providing me the foraminifera samples from his own collection which are an important aspect of my master thesis. Dr. Lennart de Nooijer for guidance and comments in general and for helping me develop the preparation procedures for the stable isotope analyses of the foraminifera. Dr. Karoliina Koho for helping me with the SEM analyses, Dr. Herman van Roermund for helping me with the Electron Microprobe-scanning electron microscope analyses and Dr. Gernot Nerkhe for performing Raman spectroscopy. Also the lab technicians Natasja Welters, Jan van Tongeren (Laboratory of Palaeobotany & Palynology) and Arnold van Dijk (Laboratory of Geochemie) for providing me excess to their Laboratories and helping me with the processing of my samples. Additionally the Palaeoecology group for providing me the necessary tools and a nice working space.

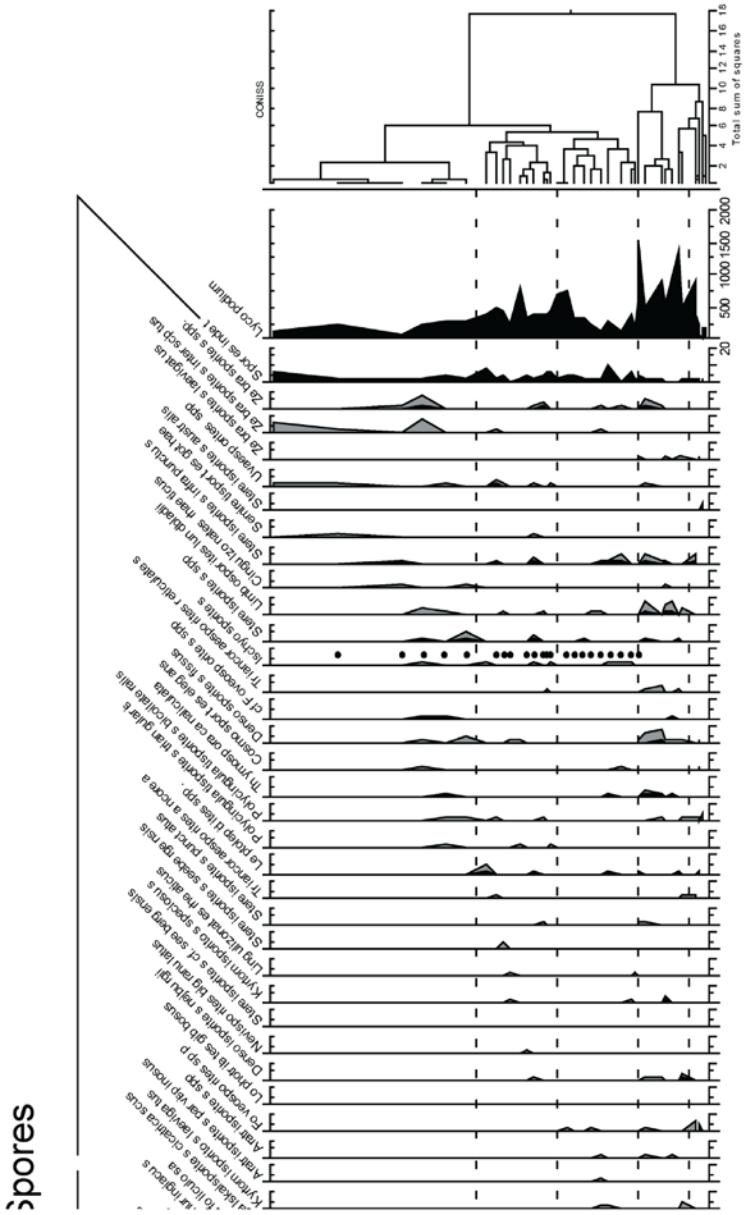
CONISS
Total sum of squares
Spores

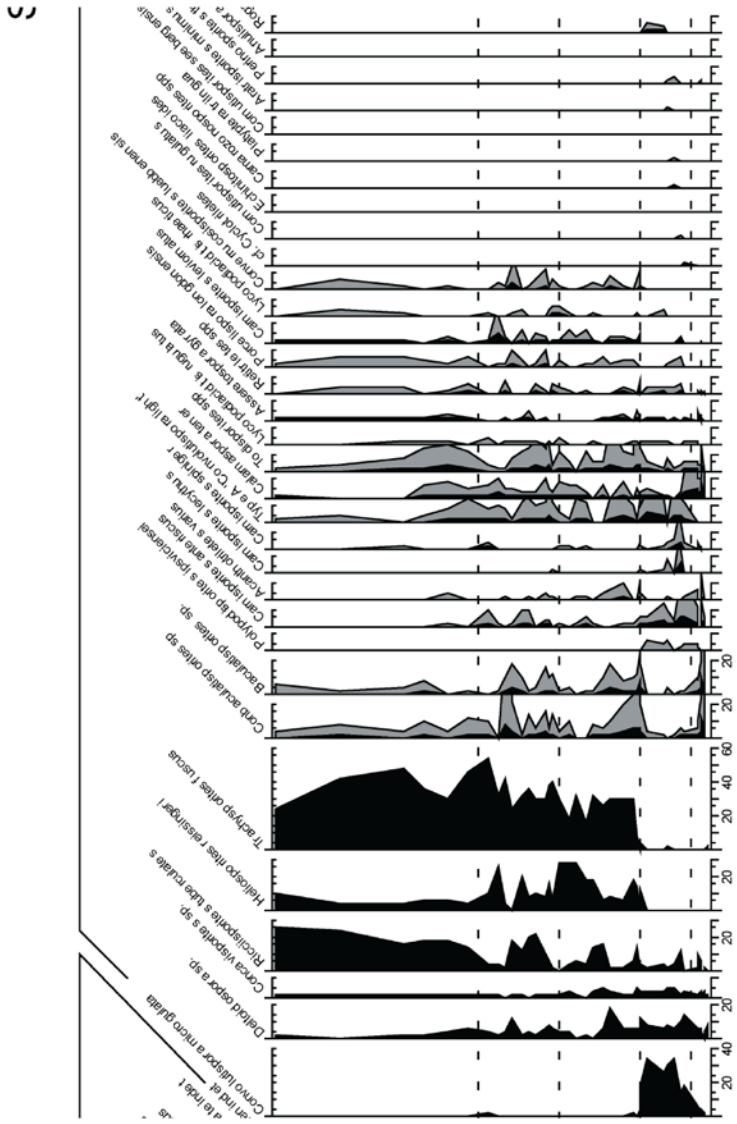

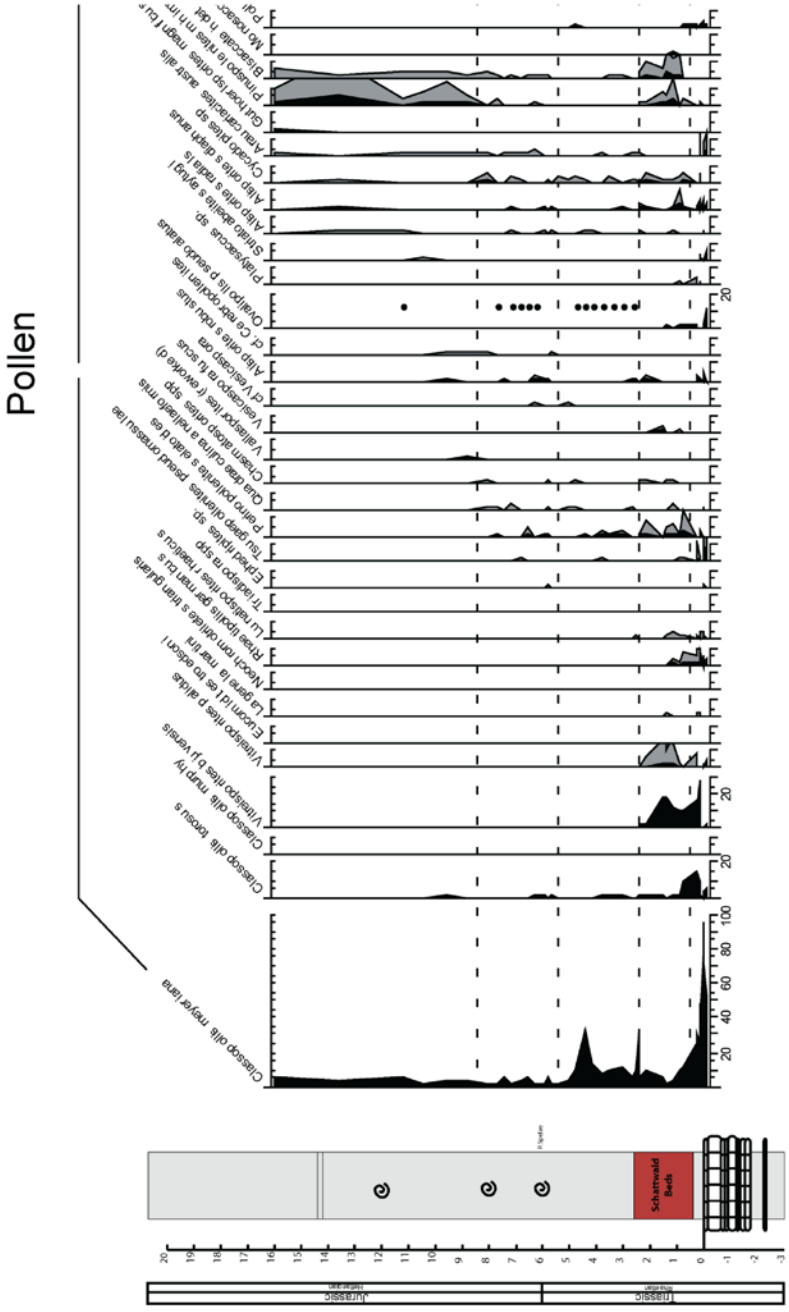

Figure 9 Relative abundances of terrestrial palynomorphs throughout the Triassic-Jurassic transition in the Kuhjoch section.

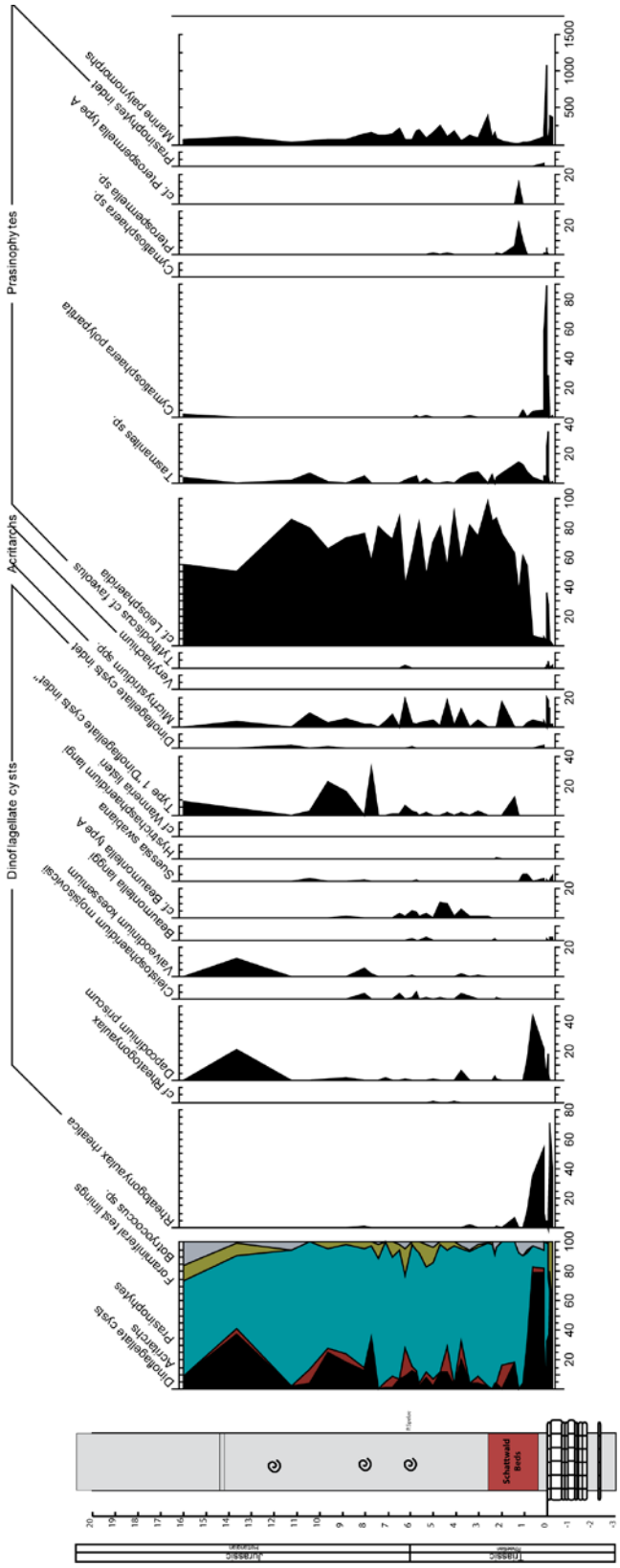

Figure 10 Relative abundances of aquatic palynomorphs throughout the Triassic-Jurassic transition in the Kuhjoch section.

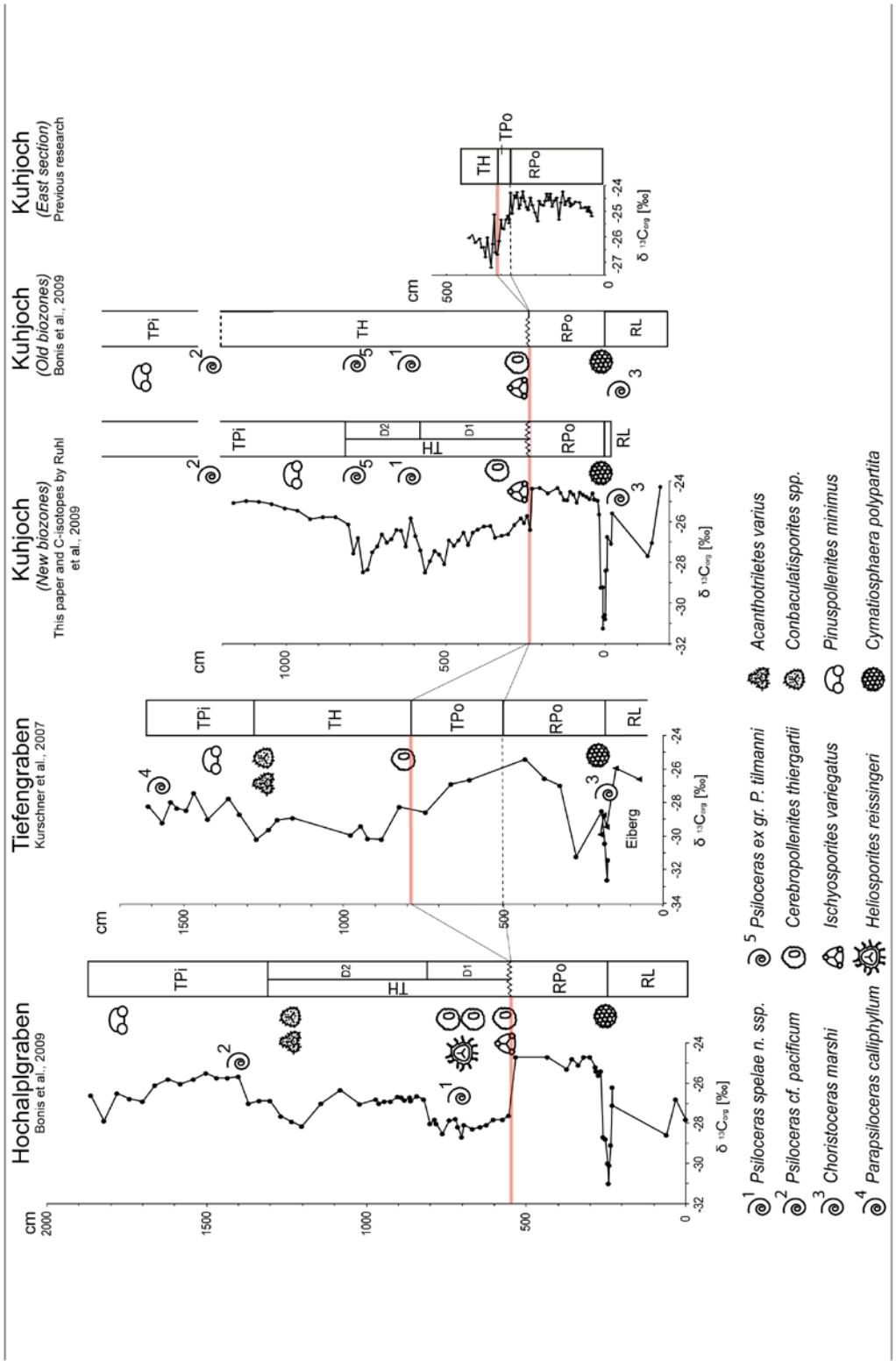

Figure 11 Correlation scheme of Hochalplgraben, Tiefengraben and Kuhjoch based on palynomorphs, palynomorph biozones, carbon-isotope stratigraphy and ammonites.

Plate 1

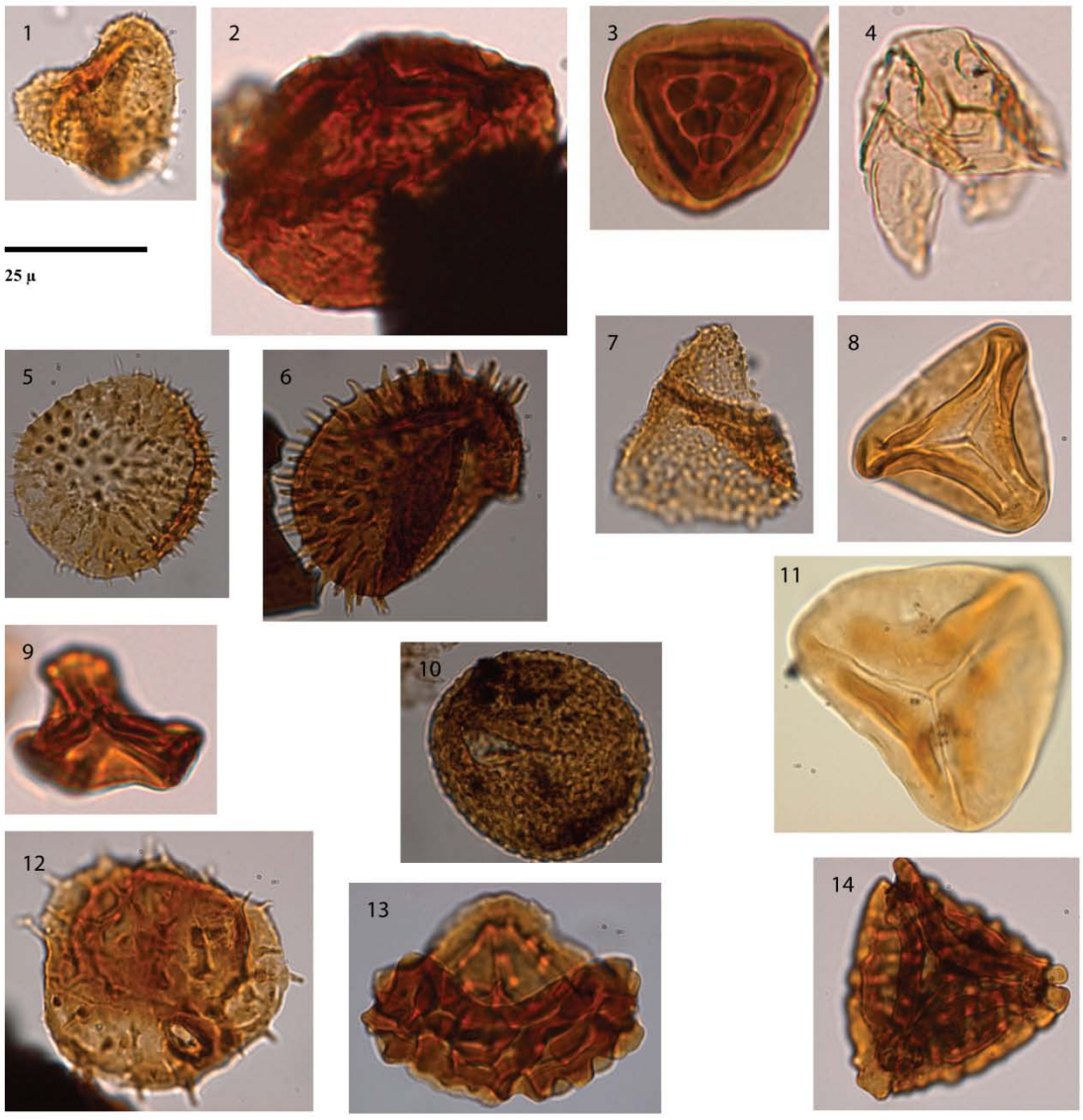

Plate 1: Spores

1) *Acanthotriletes varius* S33 (1), 96/37.8
2) *Arartrisporites parvispinosus* S37(1), 92.1/30.2
3) *Asseretospora gyrate* S29 (1), 95.7/38.2
4) *Calamaspora tener* S57 (1), 106/34.4
5) *Carnisporites anteriscus* S57 (1), 109.5/31.7
6) *Carnisporites lecythus* S22(1), 97.5/40.9
7) *Conbaculatisporites* spp. S33(1), 95.2/44.1
8) *Concavisporites* spp. S51(1), 105.7/26.2
9) *Cosmosporites elenganse*s S71 (1), 95.7/25.5
10) *Polypodiisporites polymicroforatus* S22 (1), 97.1/40.6
11) *Deltoidospora* spp. S27 (1), 100.2/25
12) *Heliosporites reissingeri* tetraether S37 (1), 112.1/41.
13) *Ischyosporites variegatus* S49 (2), 94.1/32.1
14) *Kyrtomisporis speciosus* S22 (1), 101.9/26.4

Plate 2

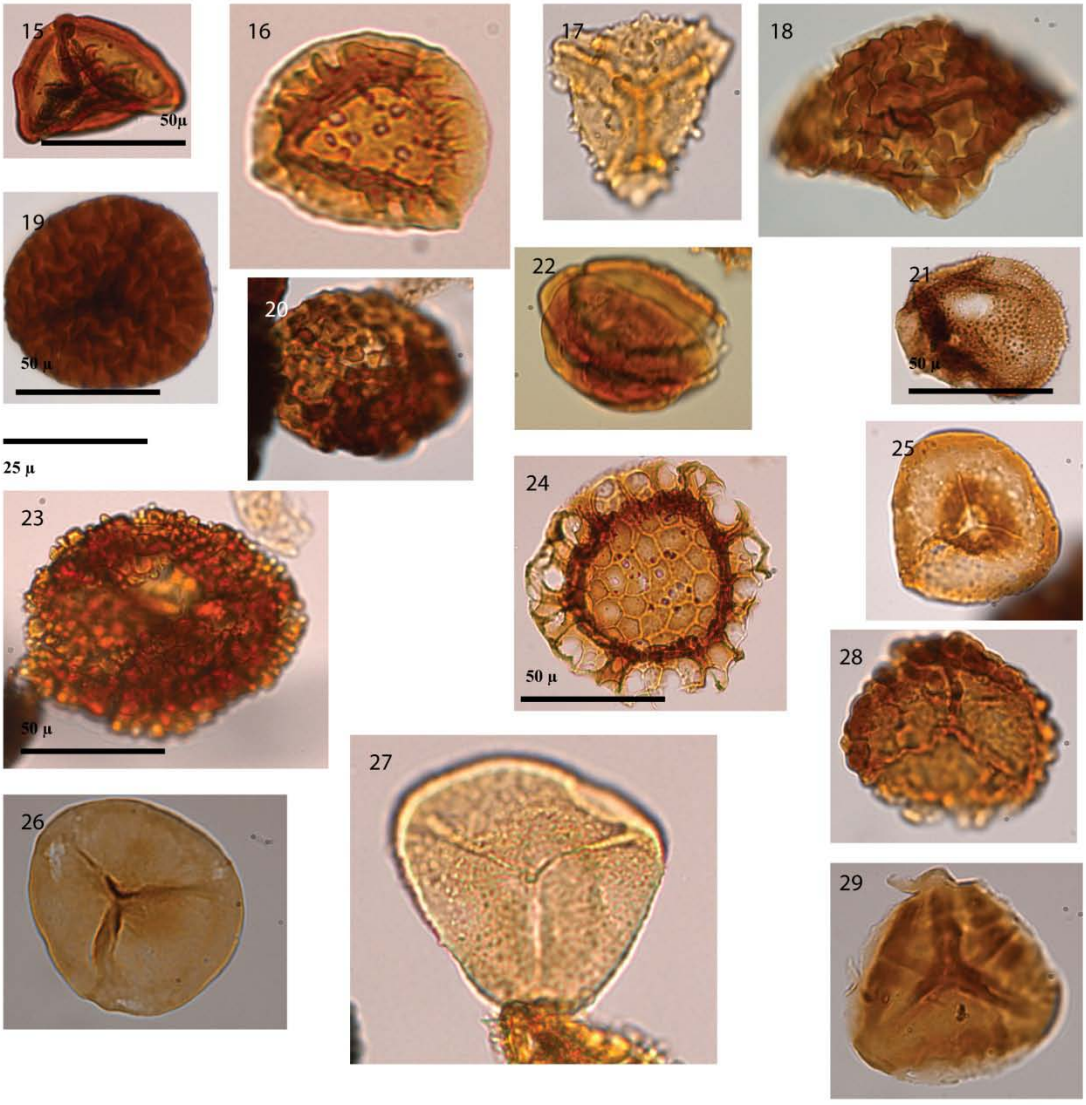

Plate 2: Spores

15) *Kyrtomisporis laevigatus* S37 (1), 98.6/32.6
16) *Limbosporites lundbladii* S61 (1), 101.7/29.5
17) *Lophotriletes* spp. S51 (1), 96/22.7
18) *Lycopodiacidites rhaeticus* S29 (1), 94.8-26.8
19) *Lycopodiacidites rugulatus* S29 (1), 97/29.1
20) *Polypodiisporites ipscievensis* S22 (1), 98.7/35.4
21) *Porcellispora longdone*nsis S18 (1), 99.6/39.5
22) *Rhaetipollis germanicus* S20 (1), 96.9/39.4
23) *Riccisporites tuberculatus* S53 (1), 100.8/45
24) *Semiretisporis gothea* S53 (1), 111/37.3
25) *Stereisporites infrapunctus* S73(1), 103.1/31.1
26) *Todisporites* spp. S51 (1), 106.1/39
27) *Trachysporites fuscus* S63 (1), 99.6/25.5
28) *Uvaesporites argentaeformis* S63 (1), 99.6/25.5
29) *Zebrasporites interscriptus* S73(1), 100.1/39

Plate 3

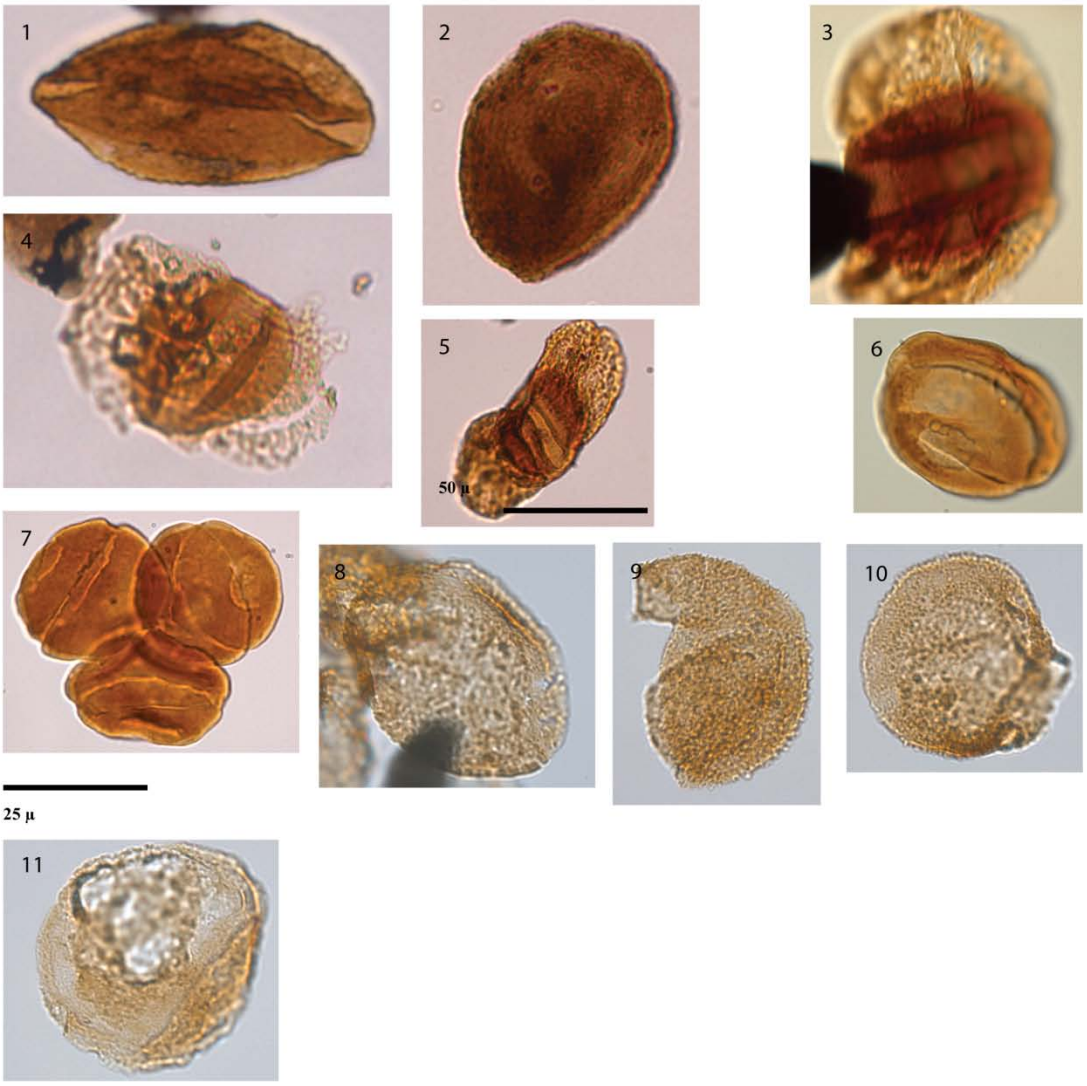

Plate 3: Pollen

1) *Cycadopites* spp. S29 (1), 97.9/32.3
2) *Lagenella martini* S22 (1), 100.7/35.4
3) *Lunatisporites rheaticus* S20 (1), 98/41
4) *Lunatisporites rheaticus* S29 (1), 97.6/34.1
5) Cf. *Plattysaccus* sp. S22 (1), 101.5/34.5
6) *Classopollis meyeriana* S35 (1), 100.2/27.4
7) *Classopollis meyeriana* tetraether S35 (1), 100.2/27.4
8) *Cerebropollenites thiergartii* S33(1), 97.1/42.6
9) *Cerebropollenites thiergartii* S35(2), 101.4/39.1
10) *Cerebropollenites thiergartii* S37 (1), 97.8/45.6
11) *Cerebropollenites thiergartii* S37(1), 98.7/44.9

Plate 4

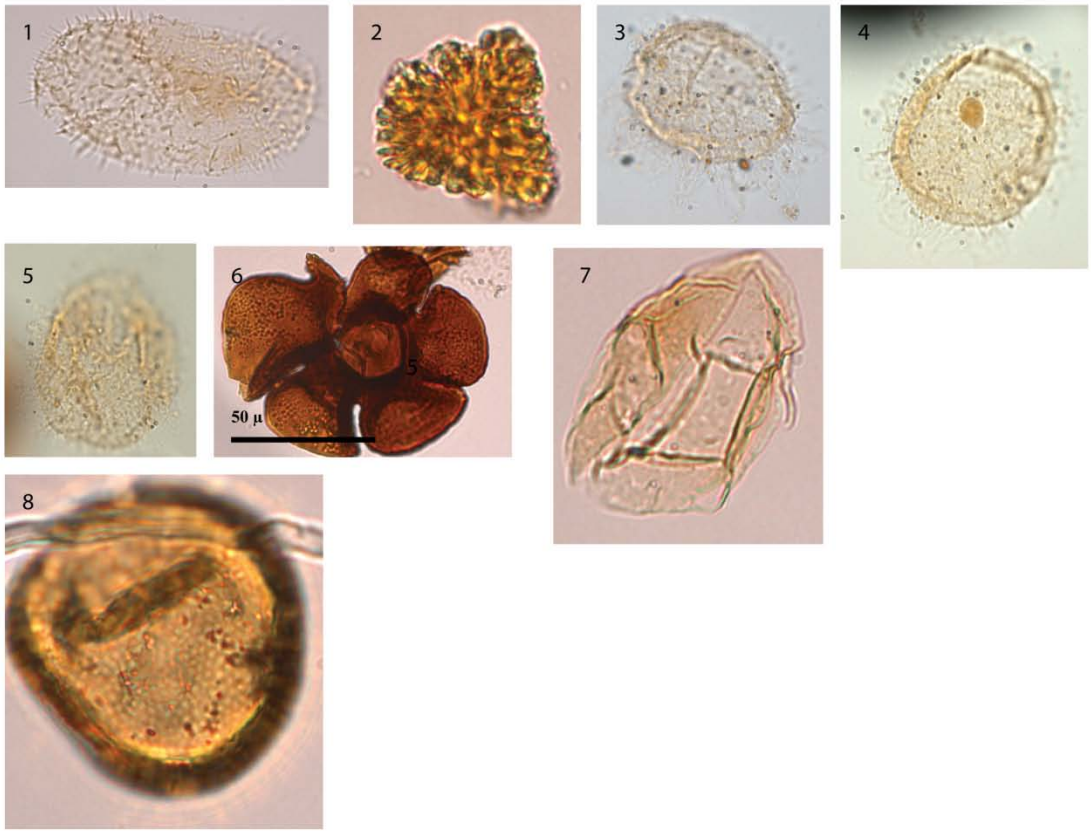

Plate 4: Aquatic palynomorphs

1) Cf. *Beaumontella* type A S37 (1), 100.5/32
2) *Botryococcus* sp. S57 (1), 111.6/26.4
3) Type 1 Dinoflagellate cyst indet S65 (2), 103.5/27.5
4) Type 1 Dinoflagellate cyst indet S65 (2), 104.8/37.7
5) Type 1 Dinoflagellate cyst indet S50 (1), 102.6/30.7
6) Foraminiferal test lining S53 (1), 110.3/44.2
7) Cf. *Leiospharidia* sp. S51 (1), 106.9/31.6
8) *Tasmanites* sp. S51 (1), 106.9/31.6

Plate 5

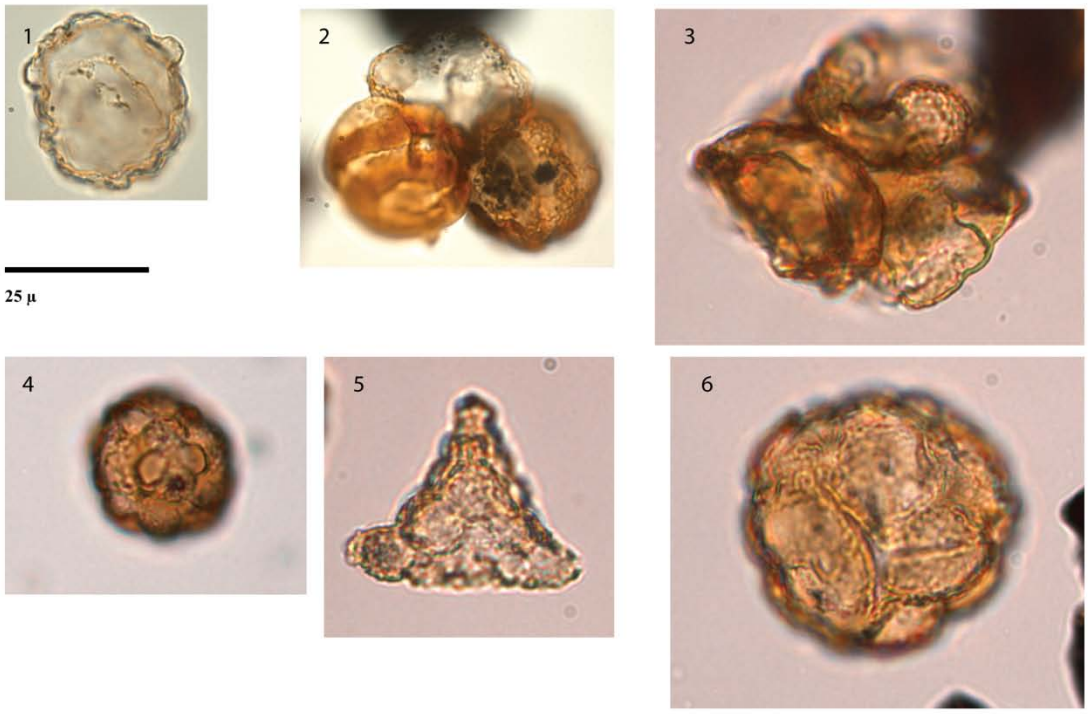

Plate 5: Deformed palynomorphs

1) small deformed pol (light) S35 (1), 100.2/36.6
2) *Classopollis meyeriana* tetraether *with one preserved specimen and two deformed specimens* cropped S35 (1), 100.3/25.8
3) Deformed tetraether S63 (1), 104.5/30.2
4) Small deformed pol (dark) S61 (1), 102.1/37
5) Deformed spore *concave triangular shape* S51 (1), 106.2/25.6
6) Deformed spore *trilete mark* S53 (1), 96.8/40.6

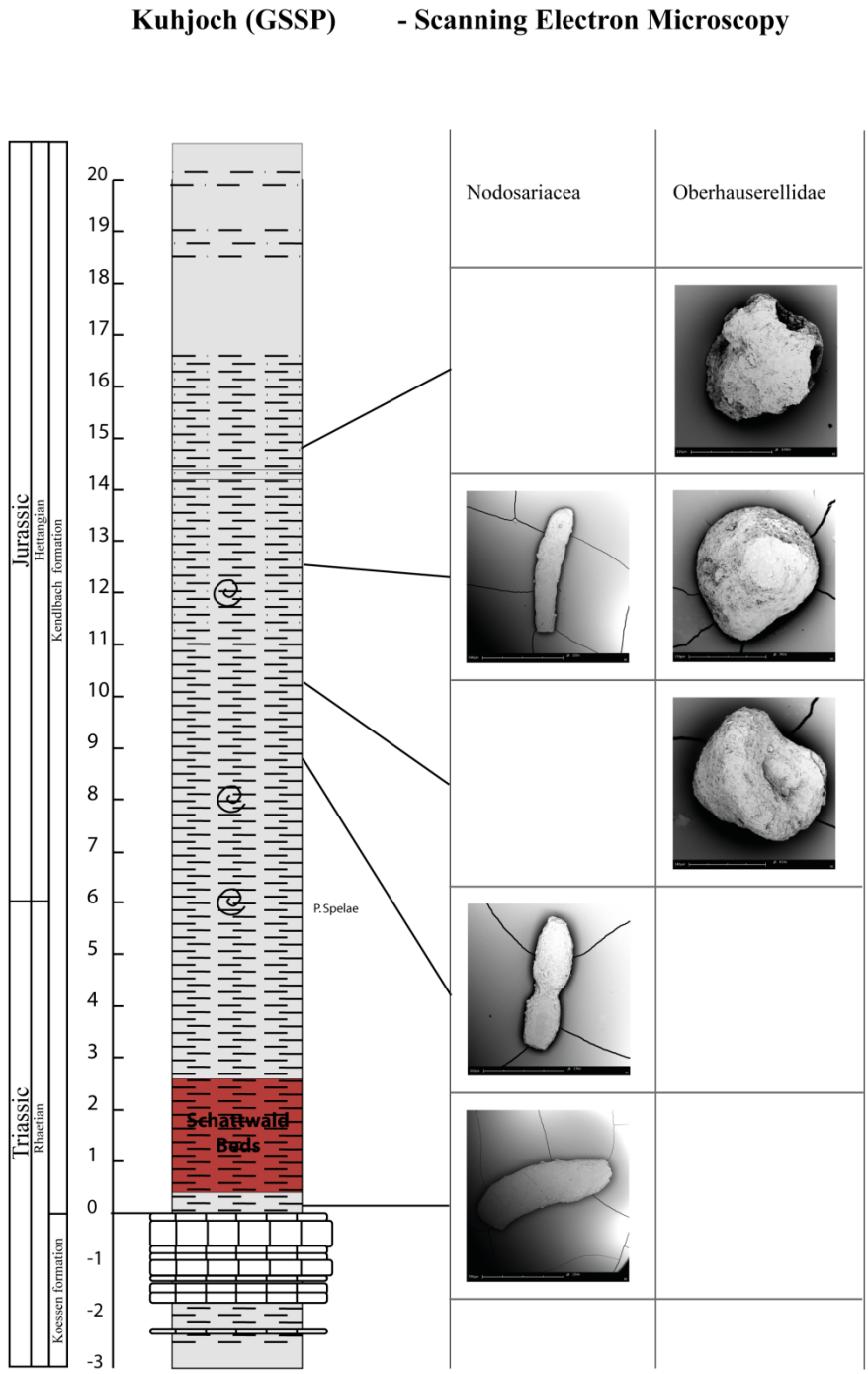

Figure 12 SEM pictures of both *Reinholdella* spp. and *Dentalina* spp. specimens from different stratigraphic heights of Kuhjoch

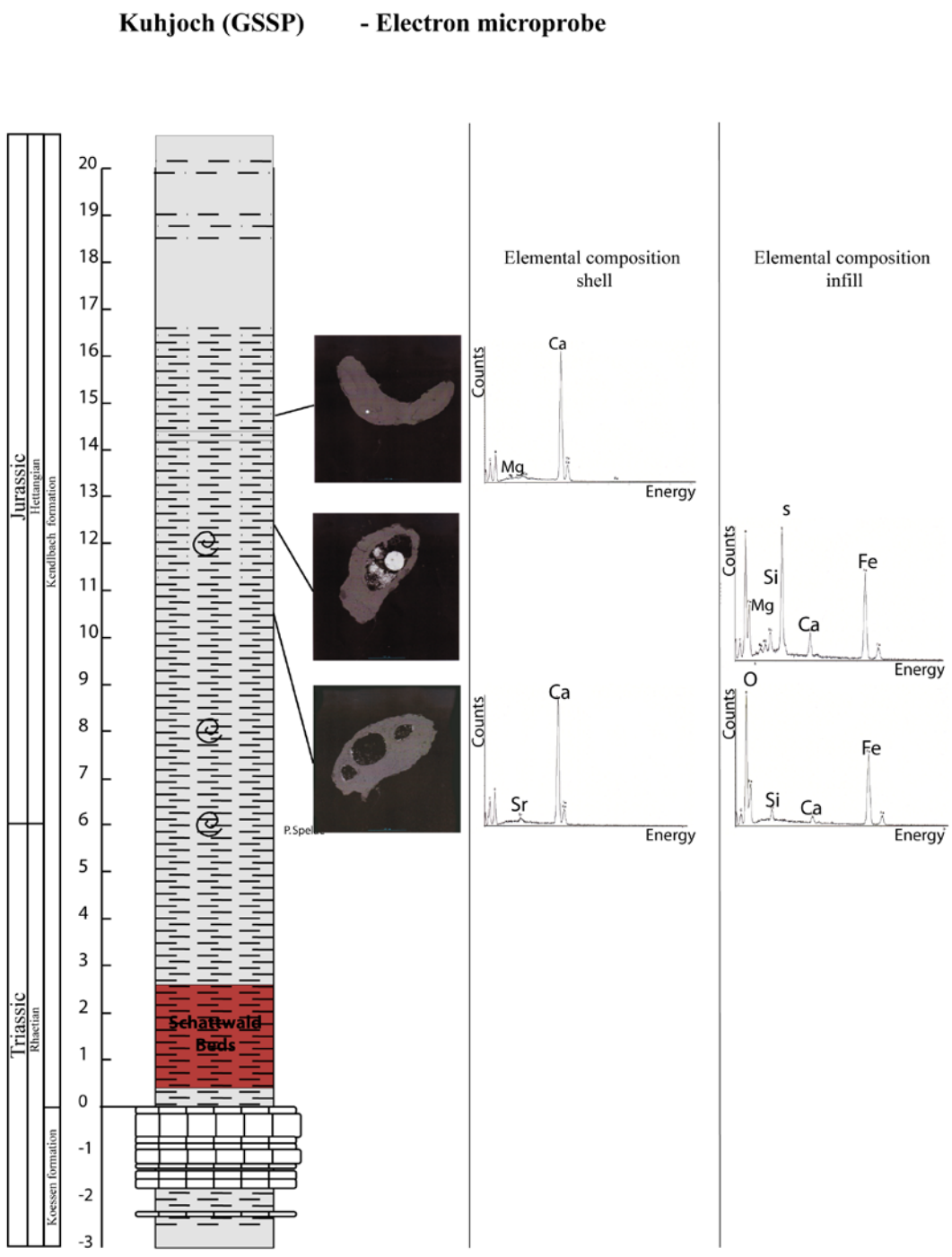

Figure 13 Electron microprobe-scanning electron microscope analyses on three *Reinholdella* spp. specimens with spectra of the elemental composition from the shell and the infill.

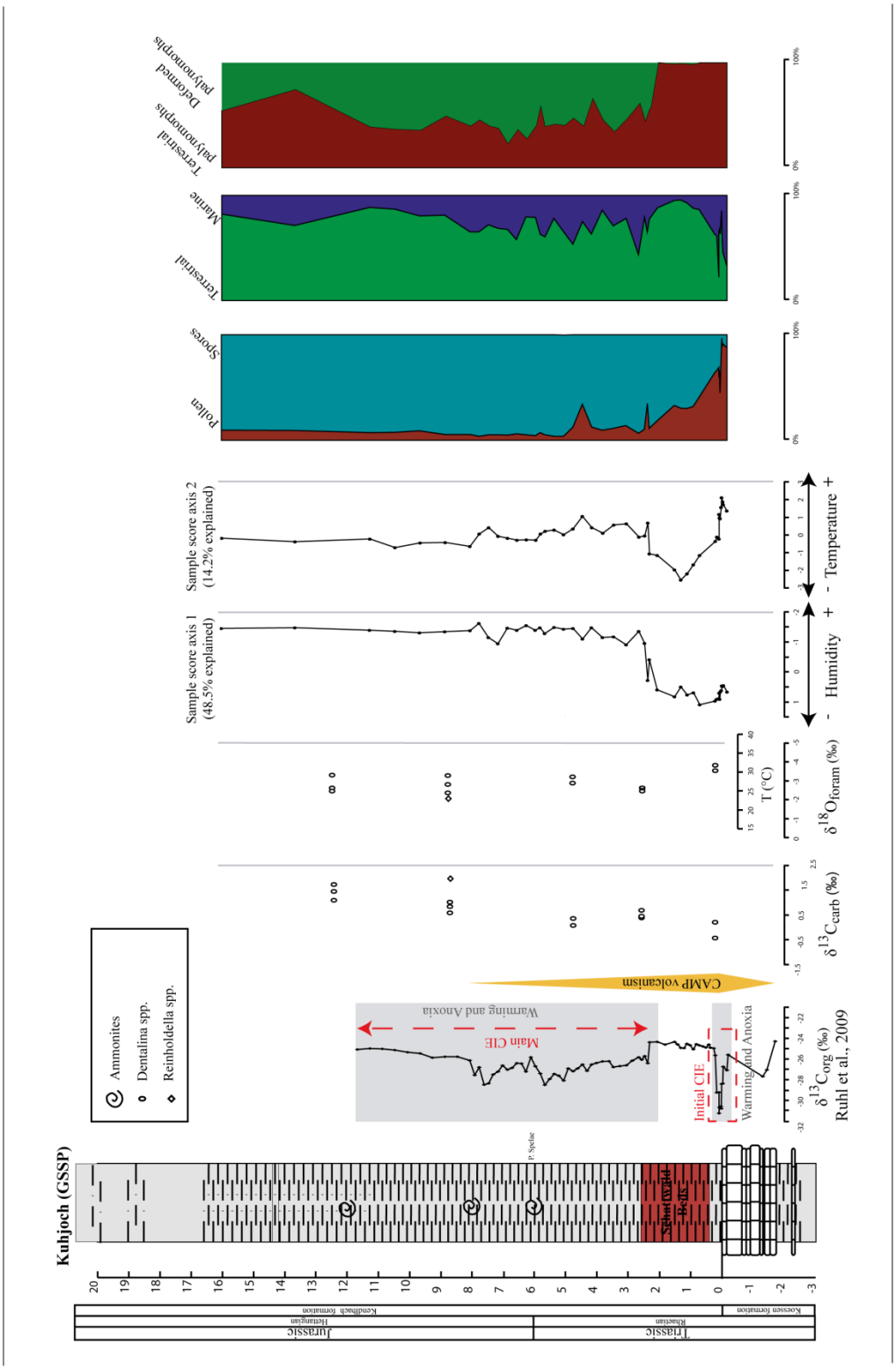

Figure 14 Lithology together with $\delta^{13}C_{org}$, $\delta^{13}C_{carb}$, $\delta^{18}O_{foram}$, sample scores of PCA and the general distribution of palynomorph assemblages.

References

Arthur, M.A., W.E. Dean & L.M. Pratt. (1988), Geochemical and climatic effects of increased marine organic carbon burial at the Cenomanian/Turonian boundary.

Beerling, D.J. & R.A. Berner. (2002), Biogeochemical constraints on the Triassic–Jurassic boundary carbon cycle event. Glob. Biogeochem. Cycles 16, pp.101–113.

Bemis, B.E., H.J. Spero, J. Bijma et al. (1998), Reevaluation of the oxygen isotopic composition of planktonic foraminifera: Experimental results and revised paleotemperature equations. Paleoceanography 13(2), pp.150-160.

Benton, M.J. & R.J. Twitchett. (2003), How to kill (almost) all life: the end-Permian extinction event. Trends in Ecology & Evolution 18(7), pp.358-365.

Bice, K.L., D. Birgel, P.A. Meyers et al. (2006), A multiple proxy and model study of Cretaceous upper ocean temperatures and atmospheric CO2 concentrations. Paleoceanography 21(2)

Bonis, N.R. & W.M. Kürschner. (in prep a), Abrupt climate change during the end-Tirassic mass extinction.

Bonis, N.R. & W.M. Kürschner. (in prep b), Vegetation history, diversity patterns, and climate change across the Triassic-Jurassic boundary. Paleobiology

Bonis, N.R., W.M. Kürschner & L. Krystyn. (2009), A detailed palynological study of the Triassic-Jurassic transition in key sections of the Eiberg Basin (Northern Calcareous Alps, Austria). Review of Paleobotany and Palynology 156, pp.376-400.

Bonis, N.R., M. Ruhl & W.M. Kürschner. (2010a), Climate change driven black shale deposition during the end-Triassic mass extinction. Palaeogeography, Palaeoclimatolegy, Palaeoecolegy 290(1-4), pp.151-159.

Bonis, N.R., M. Ruhl & W.M. Kürschner. (2010b), Milankovitch-scale palynological turnover across the Triassic–Jurassic transition at St. Audrie's Bay, SW UK. geological society 167(5), pp.877-888.

Bowen, G.J., D.J. Beerling, P.L. Koch et al. (2004), A humid climate state during the Palaeocene/Eocene thermal maximum. Nature 432(7016), pp.495-499.

Caldeira, K. & M.E. Wickett. (2003), Anthropogenic carbon and ocean pH. Nature 425, pp.365.

Chave, K.E. (1954), Aspects of the biogeochemistry of magnesium 1. Calcareous marine organisms. The Journal of geology 62(3), pp.266-283.

Deenen, M.H.L., M. Ruhl, N.R. Bonis et al. (2010), A new chronology for the end-Triassic mass extinction. Earth & Planetary Science Letters 291, pp.113-125.

Dunkley Jones, T., A. Ridgwell, D.J. Lunt et al. (2010), A Palaeogene perspective on climate sensitivity and methane hydrate instability. Philosophical Transactions of the Royal Society A: Mathematical, Physical and Engineering Sciences 368(1919), pp.2395.

Emiliani, C. (1955), Pleistocene temperatures. The Journal of geology 63(6), pp.538-578.

Fairbanks, R.G., M. Sverdlove, R. Free et al. (1982), Vertical distribution and isotopic fractionation of living planktonic foraminifera from the Panama Basin.

Forster, A., S. Schouten, K. Moriya et al. (2007), Tropical warming and intermittent cooling during the Cenomanian/Turonian oceanic anoxic event 2: Sea surface temperature records from the equatorial Atlantic. Paleoceanography 22(1)

Fowell, S.J., B. Cornet & P.E. Olsen. (1994), Geologically rapid Late Triassic extinctions: Palynological evidence from the Newark Supergroup. Geological Society of America Special Paper 288

Fowell, S.J. & P.E. Olsen. (1993), Time calibration of Triassic/Jurassic micro floral turnover, eastern North America. Tectonophysics 222, pp.361-369.

Galli, M.T., F. Jadoul, S.M. Bernasconi et al. (2005), Anomalies in global carbon cycling and extinction at the Triassic/Jurassic boundary: evidence from a marine C-isotope record. Palaeogeography, Palaeoclimatolegy, Palaeoecolegy 216(3-4), pp.203-214.

Götz, A.E., K. Ruckwied, J. Pálfy et al. (2009), Palynological evidence of synchronous changes within the terrestrial and marine realm at the Triassic/Jurassic boundary (Csovár section, Hungary). Review of palaeobotany and palynology 156(3-4), pp.401-409.

Grossman, E.L. (1987), Stable isotopes in modern benthic foraminifera; a study of vital effect. The Journal of Foraminiferal Research 17(1), pp.48.

Grossman, E.L. & T.L. Ku. (1986), Oxygen and carbon isotope fractionation in biogenic aragonite: temperature effects. Chemical Geology: Isotope Geoscience Section 59, pp.59-74.

Hallam, A. (2002), How catastrophic was the end-Triassic mass extinction? Lethaia 35(2), pp.147.

Hallam, A., J.A. Crame, M.O. Mancenido et al. (1993), Jurassic Climates as Inferred from the Sedimentary and Fossil Record [and Discussion]. Philosophical Transactions: Biological Sciences 341(1297), pp.pp. 287-296.

Hautmann, M. (2004), Effects of end-Triassic CO^2 maximum on carbonate sedimentation and marine mass extinction. Facies 50, pp.257-261.

Hautmann, M., M.J. Benton & A. Tomasovych. (2008), Catastrophic ocean acidification at the Triassic-Jurassic boundary. N. Jb. Geol. Palaeont. abh. 249(1), pp.119-127.

Hesselbo, S.P., A.M. Christopher & J. Pálfy. (2007), Triassic-Jurassic boundary events: Problems, progress, possibilities. Palaeogeography, Palaeoclimatolegy, Palaeoecolegy 244(1-10)

Hesselbo, S.P., S.A. Robinson, F. Surlyk et al. (2002), Terrestrial and marine extinction at the Triassic–Jurassic boundary synchronized with major carbon-cycle perturbation: a link to initiation of massive volcanism. Geology 30, pp.251–254.

Hillebrandt, A., L. Krystyn & W.M. Kürschner. (2007), A candidate GSSP for the base of the Jurassic in the Northern Calcereous Alps (Kuhjoch section; Karwendel Mountains, Tyrol, Austria). International subcomission on Jurassic Stratigraphy Newsletters 34, pp.2-20.

Hillebrandt, A.v. & L. Krystyn. (2009), On the oldest Jurassic ammonites of Europe (Northern Calcareous Alps, Austria) and their global significance. Geol. Paläont. Abh. 253(2-3), pp.163-195.

Hillebrandt, A.v. & M. Urlichs. (2008), Foraminifera and ostracoda from the northern calcareous alps and the end-triassic biotic crisis. Berichte Geol. B.-A. 76

Hounslow, M.W., P.E. Posen & G. Warrington. (2004a), Magnetostratigraphy and biostratigraphy of the Upper Triassic and lowermost Jurassic succession, St. Audrie's Bay, UK. Palaeogeography, Palaeoclimatolegy, Palaeoecolegy 213, pp.331-358.

Hounslow, M.W., P.E. Posen & G. Warrington. (2004b), Magnetostratigraphy and biostratigraphy of the Upper Triassic and lowermost Jurassic succession, St. Audrie's Bay, UK. Palaeogeography, Palaeoclimatolegy, Palaeoecolegy 213(3-4), pp.331-358.

Huynh, T.T. & C.J. Poulsen. (2005), Rising atmospheric CO2 as a possible trigger for the end-Triassic mass extinction. Palaeogeography, Palaeoclimatology, Palaeoecology 217(3-4), pp.223-242.

Imbrie, J., J. Hays, D. Martinson et al. (1984). The orbital theory of pleistocene climate: Support from a revised chronology of the marine delta18 O record. Paper presented at the Milankovitch and Climate: Understanding the Response to Astronomical Forcing, , 1 pp.269.

Korte, C., S.P. Hesselbo, H.C. Jenskyns et al. (2009), Paleoenvironmental significance of carbon and oxygen-isotope stratigraphy of marine Triassic Jurassic boundary sections in SW Britain. Journal of the Geological society 166, pp.431-445.

Krystyn, L., F. Boehm, W.M. Kürschner et al. (2005), The Triassic-Jurassic boundary in the Northern Calcereous Alps. In: Palfy J. and Oszvart P. (Eds), Program, Abstracts and Field Guide. 5th Field Workshop of IGCP 458 Project (Tata and Hallein, September 2005)

Kürschner, W.M., N.R. Bonis & L. Krystyn. (2007), Carbon-isotope stratigraphy and palynostratigraphy of the Triassic-Jurassic transition in the Tiefengraben section -Northern Calcereous Alps (Austria). Palaeogeography, Palaeoclimatolegy, Palaeoecolegy 244(1-4), pp.257-280.

Love, L.G. & J.W. Murray. (1963), Biogenic pyrite in recent sediments of Christchurch harbour, England. American Journal of Science 261(5), pp.433.

McCarren, H., E. Thomas, T. Hasegawa et al. (2008), Depth dependency of the Paleocene-Eocene carbon isotope excursion: Paired benthic and terrestrial biomarker records (Ocean Drilling Program Leg 208, Walvis Ridge). Geochemistry Geophysics Geosystems 9(10), pp.Q10008.

McElwain, J.C., M.E. Popa, S.P. Hesselbo et al. (2007), Macroecological responses of terrestrial vegetation to climatic and atmospheric change across the Triassic/Jurassic boundary in East Greenland. Paleobiology 33(4), pp.547-573.

Metaxas, A. & R.E. Scheibling. (1996), Top-down and bottom-up regulation of phytoplankton assemblages in tidepools. Marine Ecology Progress Series 145(1), pp.161-177.

Morbey, S.J. (1975), The palynostratigraphy of the Rhaetian stage, Upper Triassic in the Kendlbachgraben, Austria. Palaeontographica Abteilung B Paläophytologie 152, pp.1-75.

Neves, R. & H.J. Sullivan. (1964), Modification of fossil spore exines associated with the presence of pyrite cristals. Micropaleontology 10(4), pp.443-452.

Nürnberg, D., J. Bijma & C. Hemleben. (1996), Assessing the reliability of magnesium in foraminiferal calcite as a proxy for water mass temperatures. Geochimica et Cosmochimica Acta 60(5), pp.803-814.

Olsen, P.E., D.V. Kent, H.-. Sues et al. (2002a), Ascent of Dinosaurs Linked to an Iridium Anomaly at the Triassic-Jurassic Boundary. Science 296, pp.1305-1307.

Pagani, M., N. Pedentchouk, M. Huber et al. (2006), Arctic hydrology during global warming at the Palaeocene/Eocene thermal maximum. Nature 442(7103), pp.671-675.

Pálfy, J., A. Demény, J. Haas et al. (2001), Carbon isotope anomaly and other geochemical changes at the Triassic–Jurassic boundary from a marine section in Hungary. Geology 29(1047–1050)

Passier, H.F., J.J. Middelburg, G.J.d. Lange et al. (1997), Pyrite contents microtextures and sulfur isotopes in relation to formation of the younghest eastern Mediterranean sapropel. Geology 25, pp.519-522.

Pedersen, K.R. & J.J. Lund. (1980), Palynology of the plant-bearing rhaetian to hettangian kap stewart formation, scoresby sund, east greenland. Review of palaeobotany and palynology 31, pp.1.

Pisias, N.G., D.G. Martinson, T.C. Moore Jr et al. (1984), High resolution stratigraphic correlation of benthic oxygen isotopic records spanning the last 300,000 years. Marine Geology 56(1-4), pp.119-136.

Prauss, M. & W. Riegel. (1989), Evidence from phytoplankton associations for causes of black shale formation in epicontinental seas. Neues Jahrbuch für Geologie und Paläontologie, Monatshefte 11, pp.671-682.

Raup, M.D. & J.J. Sepkoski. (1982), Mass Extinctions in the Marine Fossil Record. Science 215(4539), pp.1501-1503.

Rohling, E.J. & S. Cooke. (2003). Stable oxygen and carbon isotopes in foraminiferal carbonate shells. pp. 239-258

Ruhl, M., H. Veld & W.M. Kürschner. (2010), Sedimentary organic matter characterization of the Triassic-Jurassic boundary GSSP at Kuhjoch (Austria). Earth and Planetary Science Letters 292(1-2), pp.17-26.

Ruhl, M., N.R. Bonis, G.-. Reichart et al. (in prep), Atmospheric methane injection caused end-Triassic mass extinction.

Ruhl, M., W.M. Kürschner & L. Krystyn. (2009), Triassic-Jurassic organic carbon isotope stratigraphy of key sections in the western Tethys realm (Austria). Earth & Planetary Science Letters 281(3-4), pp.169-187.

Schaltegger, U., J. Guex, A. Bartolini et al. (2008), Precise U-Pb age constraints for end-Triassic mass extinction, its correlation to volcanism and Hettangian post-extinction recovery. Earth and Planetary Science Letters 267(1-2), pp.266-275.

Schootbrugge, B.v.d., F. Tremolada, Y. Rosenthal et al. (2007), End-Triassic calcification crisis and blooms of organic-walled 'disaster species'. Palaeogeography, Palaeoclimatolegy, Palaeoecolegy 244, pp.126-141.

Schouten, S., E.C. Hopmans, A. Forster et al. (2003), Extremely high sea-surface temperatures at low latitudes during the middle Cretaceous as revealed by archaeal membrane lipids. Geology 31(12), pp.1069.

Schouten, S., M. Woltering, W.I.C. Rijpstra et al. (2007), The Paleocene-Eocene carbon isotope excursion in higher plant organic matter: Differential fractionation of angiosperms and conifers in the Arctic. Earth and Planetary Science Letters 258(3-4), pp.581-592.

Schuurman, W.M.L. (1979), Aspects of late Triassic palynology. 3. Palynology of latest Triassic and earliest Jurassic deposits of the northern limestone alps in Austria and southern Germany, with special reference to a palynological characterization of the Rhaetian stage in Europe. Review of Palaeobotany and Palynology 27(1), pp.53-57.

Sepkoski, J.J. (1982), Mass extinctions in the Phanerozoic oceans: A review. Geological Society of America Special Paper 190, pp.283-289.

Shackleton, N.J. & N.D. Opdyke. (1973), Oxygen isotope and palaeomagnetic stratigraphy of Equatorial Pacific core V28-238: Oxygen isotope temperatures and ice volumes on a 105 year and 106 year scale* 1. Quaternary Research 3(1), pp.39-55.

Spicer, R.A., P.M. Rees, J.L. Chapman et al. (1993), Cretaceous Phytogeography and Climate Signals [and Discussion]. Philosophical Transactions: Biological Sciences 341(1297), pp.pp. 277-286.

Srivastava, S.C., A.K. Srivastava, A.P. Bhattacharyya et al. (1999), Degraded Permian Palynomorphs from North-East Himalaya, India. Note to Readers: Cyrillic Fonts used in the Russian text in this issue are shown as? marks.We were unable to get the computer to translate the font.We are sorry for the inconvenience., pp.32.

Tappan, H. (1980). The paleobiology of plant protists. pp. 1028. San Francisco: W. H. Freeman.

Thomas, E. (2007), Cenozoic mass extinctions in the deep sea: What perturbs the largest habitat on Earth? Large Ecosystem Perturbations: Causes and Consequences, pp.1–24.

Tiwari, R.S., B.K. Misra & K.L. Meena. (1990), Pyritic degradation of palynomorphs in Early triassic assemblage from Raniganj coalfield, West Bengal. Indian J. Geol. 62, pp.88-95.

Tyson, R.V. (1995). Organic facies and palynofacies. Sedimentary organic matterpp. 615. London: Chapman & Hall.

Vakhrameev, V.A. (1987), Climates and the distribution of some gymsosperms in Asia during the Jurassic and Cretaceous. Review of palaeobotany and palynology 51(1-3), pp.205-212.

Ward, P.D., G.H. Garrison, K.H. Williford et al. (2007), The organic carbon isotopic and paleontological record across the Triassic-Jurassic boundary at the candidate GSSP section at Ferguson Hill, Muller Canyon, Nevada, USA. Palaeogeography, Palaeoclimatolegy, Palaeoecolegy 244(1-4), pp.281-289.

Ward, P.D., J.W. Haggart, E.S. Carter et al. (2001), Sudden productivity collapse associated with the Triassic–Jurassic boundary mass extinction. Science 292, pp.1148–1151.

Weis, W., J.H. Brown, S. Cusack et al. (1988), Structure of the influenza virus haemagglutinin complexed with its receptor, sialic acid.

Wilkin, R.T., H.L. Barnes & S.L. Brantley. (1996), The size distribution of framboidal pyrite in modern sediments: An indicator of redox conditions. Geochimica et Cosmochimica Acta 60(20), pp.3897.

Williford, K.H., P.D. Ward, G.H. Garrison et al. (2007), An extended organic carbon-isotope record across the Triassic-Jurassic boundary in the Queen Charlotte Islands, British Columbia, Canada. Palaeogeography, Palaeoclimatolegy, Palaeoecolegy 244, pp.290-296.

Zachos, J.C., S. Schouten, S. Bohaty et al. (2006), Extreme warming of mid-latitude coastal ocean during the Paleocene-Eocene Thermal Maximum: Inferences from TEX86 and isotope data. Geology 34(9), pp.737.

Zachos, J., M. Pagani, L. Sloan et al. (2001), Trends rythms, aberrations in global climate 65 Ma to present. Science 292, pp.686-693.

Zachos, J., U. Rohl, S.A. Schellenberg et al. (2005), Rapid acidification of the ocean during the Paleocene-Eocene thermal maximum. Science 308(5728), pp.1611-1615.